Development of Test Bench for the Characterization of Shape Memory Alloy Wire

By

Haroon Ahmed Khan

NUST201463133MSMME62214F

Supervisor

Dr. Mushtaq Khan

School of Mechanical and Manufacturing Engineering National University of Science and Technology Islamabad, Pakistan

CERTIFICATE OF ORGINALITY

The substance of this thesis is the original work of the author and due reference and acknowledgement has been made, where necessary, to the work of others. No part of this thesis has been already accepted for any degree, and it is not being currently submitted in candidature of any degree.

Haroon Ahmed Khan
(NUST201463133MSMME62214F)

Thesis Scholar

Countersigned

Dr. Mushtaq Khan

Thesis Supervisor

ACKNOWLEDGEMENT

All praises and humble thanks are to Almighty ALLAH who gave me the valor and strength for successful completion of such a momentous work. No intellectual findings are the result of works of authors only; it includes also the precious contributions of others, which pave the path of success and immortality. Same is true for this MS dissertation work. There are many people who helped and supported me along the way and to whom I feel grateful.

My deep gratitude goes to my MS supervisor Dr. Mushtaq Khan for his initiation and supervision of this study and for his continuous support and engagement in the project. The efforts and supreme guidance of Dr. Mushtaq Khan made it possible for me not only to serve the purpose but also to enhance my research skills as well. I am very grateful for his inspiration and guidance.

The influence of the Guidance and Examination Committee (GEC), comprising of Dr. Liaqat Ali, Dr. Hussein Imran and Dr. Emad ud din is greatly recorded. They inspired in me the taste of research and always encouraged and guided me during the course of current research.

I specially owe my deep gratitude to Dr. Jawad Aslam for sharing his knowledge, his valuable criticisms, fruitful discussions and continuous guidance and support.

Finally, and most importantly, I would like to express my warmest appreciation to my family and friends. Throughout this process, it has been a comforting feeling to have the support of loved ones that show genuine interest in my world.

Author

Contents

List of Figures

Abstract

Shape Memory Materials (SMMs) are the type of materials that memorize their shape and retain their shape when certain external force interacts with them. Shape Memory Alloys (SMA) are important member of shape memory materials class and they come back to their programmed shape when subjected to magnetic or thermomechanical variations. Over the past few decades, shape memory alloys have gained great significance and they are now being used in biomedical, robotics, aerospace and many other industrial applications. Nitinol is an equiatomic alloy containing Nickel and Titanium and it is the best shape memory alloy among all the polycrystalline shape memory alloys. Different techniques have been used to find the characteristics of shape memory alloys. In this thesis a test bench is developed along with the software for the testing of Nitinol wire using different sensors and actuators.

Nitinol retains its programmed shape when it is subjected to Joule Heating. In order to find the properties of Nitinol wire when it is Joule heated, a software is developed. LabVIEW 2015 that is user friendly and easy to interface with hardware is used for the development of software. A Nitinol wire is pre-loaded and then Joule heated and the characteristics of the wire are obtained with the help of different sensors and the software. The results are validated by comparing with other researches and different experiments are performed that gives the relationship between displacement and the applied stress.

Chapter 1

Introduction

1.1 Introduction:

There has been a rapid growth in the field of science and technology for the last few decades. The world is going towards automation and smart/intelligent systems with the help of actuators, sensors and micro-controllers. Different sensors are being developed and smart materials are in great demand for this purpose. Such materials exhibit changes when physical interaction is made. A change in environment is sensed by smart materials and some reaction is shown in response to that change[1]. Shape memory alloys (SMAs), piezoelectric materials, magnetostrictive materials and electrostrictive materials are some of the examples of smart materials.

Shape memory alloys can be defined as a group of metallic alloys that come back to original shape and size from the deformation caused by temperature or the magnetic field. Two exceptional properties shown by shape memory alloys are:

1. Shape memory Effect
2. Superelasticity

Shape memory means the recovery of shape from the deformation caused by heating SMA above its transformation temperature. The recovery of strain during mechanical loading and unloading at temperature greater than SMAs' transformation temperature is called superelasticity[2]. This recovery is isothermal in nature.

Many shape memory alloys have been discovered so far and still a lot of work is being done on it. Shape memory alloys have different compositions such as copper alloys, iron based alloys and nickel-titanium based alloys. The nickel-titanium NiTi based alloys are the best shape memory alloys and they exhibit best shape memory and superelasticity properties. One of the member of this family is Nitinol in which both nickel and titanium have almost equal percentage. It was discovered in early 1960s. Biocompatibility, fatigue resistance and corrosion resistance are the characteristics that make NiTi superior to other SMAs.

The two main phases of shape memory alloys are:

1. Austenite Phase (High Temperature Phase)
2. Martensite Phase (Low Temperature Phase)

Shape memory effect and superelasticity occur from martensitic transformations in shape memory alloys. By changing temperature or stress, changes are made in crystalline structure of the material. In order to find these changes and their relation with the pre-loading, current and heating rate, a test bench is developed. Different sensors are used with the help of LabVIEW 2015 that is easy to integrate with hardware devices.

1.2 Aim:

The main aim of this research is to develop a test bench that is used to find the relationship of change in SMA wire with pre-loading, current and the heating rate. Optimum current and heating rate are determined and using these values, a relationship is developed between change in length and pre-loading.

1.3 Objectives:

The main objectives of this research are:

1. To develop a test bench that is capable of measuring shape memory alloy material properties.
2. To install SMA wire, actuator and different sensors in the test bench and to calibrate them.
3. To integrate these actuators and sensors with LabVIEW 2015 using DAQ assistant and develop a program to find out the results.
4. To implement PID Control on the linear actuator using LabVIEW 2015 to maintain the pre-loading of the SMA wire.
5. To find the optimum current and heating rates on which shape memory alloys maximum change in their properties.

6. To find the relationship between change in properties and the pre-loading of the wire.

1.4 Research Methodology:

This thesis mainly comprises of: Introduction, literature review, material properties of shape memory alloys, software development, experiments for determining optimum current and heating rates, experiments on SMA wire to find relation between change in length and pre-loading and comparison with results from other research papers. The main concern in this section is the research methodology that is carried out in this thesis.

A thorough literature review was done in which shape memory alloys were studied. The working and characteristics of shape memory alloys were studied. Nitinol, the nickel-titanium alloy was selected for detailed study and later it is used for the experiments to be carried out. Nitinol wire was imported from Dynalloy, Inc. USA. Similarly, linear actuator CAHB-10 series of SKF, linear variable differential transformer (LVDT) from RS and S-type load cell were also imported.

This research was carried out in three parts. First of all literature review was done and a test bench was made on CNC machine using acrylic. Actuator and sensors were mounted on the test bench. Shape memory wire of 100 mm length and 0.5 mm diameter was mounted on the test bench with both ends tied to the supports. A special gripper was made with the help of CNC machine and wire cut machine for holding the wire.

In second part, a software was developed in LabVIEW 2015. The actuator and sensors were integrated with LabVIEW 2015 with the help of DAQ assistant. The actuator was operated with the help of a driving IC. PWM was given to the actuator and it was controlled through the software. Sensors were calibrated in this part. A circuit was developed which was used for joule heating of the wire. PID Control was implemented on the linear actuator in order to maintain the pre-loaded stress on the SMA wire.

In the third part, experiments were carried out on the SMA wire. Firstly SMA wire was heated to 500 C and then quenched in water. After the annealing of the wire, experiments were done. SMA

wire was heated at different heating rates and current values keeping the pre-loading on the wire constant. These results were analyzed and optimum heating rate and current value are selected for the actuation in the wire. Both these values are then kept constant and pre-loading on the wire was varied. These results were saved and then analyzed to find the look up table that gave us relationship between pre-loading and the actuation of the wire. Each experiment was repeated three times and results were saved in Microsoft excel file.

1.5 Thesis Outline:

There are six chapters of the thesis.

In chapter 2 a thorough literature review is done. General information of Smart materials and their types are discussed. Shape memory alloys that are a type of smart materials are described. Different types of shape memory alloys are discussed including Nitinol which has best super-elastic and shape memory properties.

Chapter 3 includes the development of test bench for characterization of shape memory alloy wire. The sensors and linear actuator that are used in the test bench are described. The sensors and actuator are thoroughly discussed in this chapter.

In chapter 4 the selection and development of software is discussed. The software is thoroughly explained and then the code is described. The execution of code is also discussed in this chapter.

Chapter 5 explains the experimentations and results. The results are first validated with the results of a research paper. The input values are selected on the basis of initial experiments and final experiments are performed to find the relationship between pre-loading and displacement.

Chapter 6 discusses the conclusions and future recommendations.

CHAPTER 2

Literature Review

2.1 Introduction:

The development of shape memory alloy was done in the mid of 20th century. Arne Olander[3] was the one who first discovered shape memory alloy (SMA), also known as “Smart Alloy”, in 1932. He was a Swedish physicist who found that gold-cadmium (Au-Cd) alloys come back to their original configuration when heated after being deformed at low temperature. In 1938, Greninger and Mooradian found the shape memory effect for copper-zinc (Cu-Zn) and copper-tin (Cu-Sn) alloys[4]. The name “shape memory” was first used by Vernon in 1941[5]. Kurdjumov and Khandros[6] elaborated the martensite phase in 1949 and same was studied by Chang and Read[7] in 1951. In the 1950’s, these affects were observed in many different alloys. William Buehler discovered the Nickel-Titanium (NiTi) shape memory alloy in 1959 but shape memory alloys were not given much importance until 1962 when William Buehler and Frederick Wang described the shape memory effect in nickel titanium alloy (NiTi)[8, 9]. It is also known as Nitinol as it has almost equal quantity of nickel and titanium in its composition[10].
Shape Memory Alloy was successfully used for a commercial application in 1969. The Grumman Aerospace Corporation used the Raychem Corporation CryoFit “shrink to fit” pipe coupler for F-14 Jet Fighter[9]. After getting recognition as a smart material, SMAs got great significance and are being used in various fields such as bio-medical[11, 12], robotics[13], mini actuators[14], aerospace[15, 16], structure and composites[17] and in micro-electromechanical systems[11]. Shape memory alloys have different compositions such as copper alloys, iron based alloys and nickel-titanium based alloys. There are also some other forms of shape memory alloys such as high temperature shape memory alloys (HTSMAs), magnetic shape memory alloys (MSMAs), SMM thin film (e.g. NiTi thin film) and shape memory polymers (SMPs)[18]. Each of them has its own advantages and are used depending upon the nature of the application. Nitinol (NiTi) is so far the best shape memory alloy in terms of its properties, shape memory and superelasticity, among all the known polycrystalline shape memory alloys.

2.2 Shape Memory Alloys (SMA):

Smart Materials are in great demand as the technology is advancing. Shape Memory Alloys (SMA) are a type of smart materials that memorizes its shape, as it can be judged by the name. Shape Memory Alloys are a group of metallic alloys that changes its shape and memorizes it. They come back to their original form when they are stimulated by the memorization process i.e magnetic field or the heating.

2.2.1 Types of Shape Memory Alloys:

There are a few types of shape memory alloys.

1. Nickel Titanium Shape Memory Alloys (NiTi)
2. Copper based Shape Memory Alloys
3. Iron based Shape Memory Alloys

Copper and Iron based shape memory alloys are readily available in the market as they are low in price but they are highly instable, brittle and their thermomechanical performance is poor. On the other hand Nickel-Titanium based shape memory alloys are very much in demand. NiTi shape memory alloys have 50 % nickel and 50 % titanium and are mostly preferred due to better properties.

2.2.2 Advantages of Shape Memory Alloys:

Shape memory alloys are significantly used for actuation processes. SMA actuators are very much better than the conventional actuators that are pneumatic, hydraulic actuators and electric motors. They are far better technologically and have excellent opportunity to replace them. SMAs can be actuated by the environmental conditions so SMA actuators can be cheaper and more advanced in mechanical structure and sizes[19]. Shape memory alloy actuators are applied in low frequency vibration and actuation applications. NiTi shape memory alloy is bio compatible as it has high resistance to wear. NiTi SMA also provides significant displacement and forces when used in actuation processes.

2.2.3 Limitations of Shape Memory Alloys:

There are a few limitations[20] in using shape memory alloys as actuators which are as follows:

1. Small usable strain
2. Low actuation frequency
3. Low controllability
4. Low accuracy

The main challenge that needs to be overcome is the low operational frequency of shape memory alloys which have comparatively high heat capacity and density. Due to this, narrow bandwidth problem occurs and shape memory alloy takes more time in transferring the heat in and out of the active element. Similarly the actuator response is effected by the shape and size of the actuator[21]. SMA actuators made of small diameter wire heat faster as they have higher resistivity. Similarly they cool faster as their surface to volume ratio is high[22].

2.3 Phases of Shape Memory Alloys:

Generally two different phases are found in shape memory alloys.

1. Austenite Phase
2. Martensite Phase

The three types of crystalline structures shown during these two phases[23]:

1. Twinned Martensite
2. Detwinned Martensite
3. Austenite

The martensite structure exists at lower temperature or room temperature and it is stable there. Similarly austenite structure exists at higher temperatures and remains stable there. Shape memory alloys start to change their phase from martensite to austenite when they are heated and their temperature is raised. The temperature at which this transformation begins is the austenite start temperature (A_s) and the temperature where this transformation completes is the austenite finish temperature (A_f). When a shape memory alloy is heated and its temperature

passes the austenite start temperature, it starts to contract and changes to austenite structure. This transformation process can also be done by applying higher loads. There comes a point when heating the shape memory alloy does not cause any change in its properties. This is the highest temperature and no more stress can be induced in the SMA at this temperature known as M_d. Heating the shape memory alloy above this temperature can cause permanent deformation in it. Once the heating is stopped, the shape memory alloy starts to come back to martensite phase from the austenite phase. The temperature at which austenite starts to transform back to martensite phase is martensite start temperature (M_s) and the temperature where this transformation completes is the martensite finish temperature (M_f).

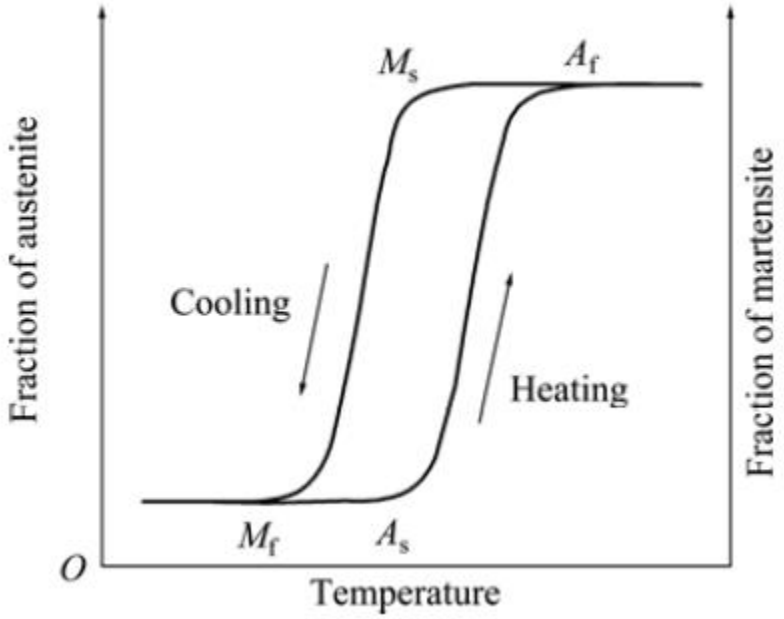

Fig. 1 Schematic Diagram of SMA thermal hysteresis

2.4 Pseudoelasticity and Shape Memory Effect:

Shape Memory Alloy recovers to its original form after being deformed by heating over the transformation temperature. At high temperature, the deformation can be recovered by

releasing the load. These transformation characteristics of shape memory alloys are known as shape memory effect and pseudoelasticity. It is either due to the phase transformation or the reorientation among martensitic variants.

2.4.1 Characterization of Shape Memory Effect:

Shape memory effect is due to thermo-elastic transformation. It is a reversible process and can be characterized as:

1. One way shape memory effect
2. Two way shape memory effect
3. Pseudoelasticity

1. **One way shape memory effect:**

   Shape memory alloy keeps the deformed shape when it is at normal temperature and returns to its original shape when it is heated.

2. **Two way shape memory effect:**

   In two way shape memory effect, the shape memory alloy retains its specific shape at both low and high temperatures. It usually provides half of the recovery strain as compared to one way shape memory effect[2].

3. **Pseudoelascticity:**

   The shape memory alloy comes back to its original shape when mechanical loading is applied keeping the temperature between A_f and M_d.

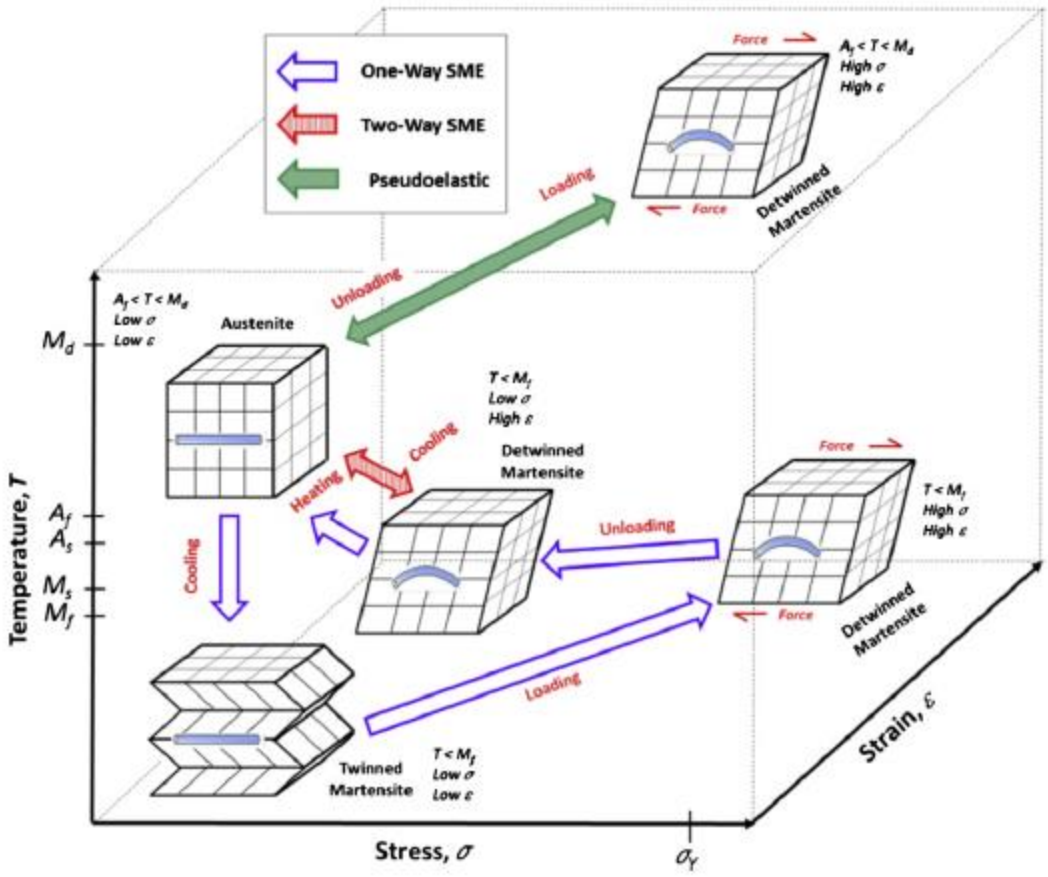

Fig. 2 SMA Phases and Crystal Structure [11]

2.5 Thermoelectric Behavior of NiTi Shape Memory Alloy:

Shape memory alloys exhibit two phases that are martensite and austenite. SMAs transform from one phase to another when they are subjected to some physical interaction. Shape memory alloys can be actuated in two ways.

1. Magnetic Field
2. Heating

The iron based shape memory alloys can be stimulated with the magnetic field and they transform from one phase to another whereas in non-ferrous shape memory alloys, including NiTi SMA,

heating is required to change the phase of SMA. Once the temperature of SMA increases above the transformation temperature, the martensitic phase converts into the austenite phase.

Nickel-Titanium shape memory alloy has the best properties among all the crystalline shape memory alloys and a lot of work is being done on NiTi shape memory alloy[24].

Many researchers have been working to find the characteristics of NiTi SMA. T Georges, V Brailovski and P Terriault developed a test bench in order to characterize and design the shape memory alloy actuators[25]. They described the antagonistic configuration of shape memory alloy actuators. Different characterization modes were discussed and force stroke characteristics of shape memory alloy actuator are obtained experimentally and analytically. 1 mm diameter shape memory alloy wire was used for experimental purposes in the test bench and two way shape memory effect was implemented as two SMA wires were used to obtain antagonistic configuration.

Some researchers have also worked to find the relationship between the electrical resistance of shape memory alloy and the stress applied. Hunter Song, Eric Kubica, and Rob Gorbet made a model in order to investigate the effects of temperature, stress and martensite phase fraction on the electrical resistance of NiTi Shape memory alloy wire during the Joule Heating[26]. A mathematical model was presented that describes the behavior of electrical resistance of shape memory alloy during the joule heating. The results were then verified by doing experiments on 0.254 mm diameter wire.

Similarly H. N. Bhargaw, M. Ahmed and P. Sinha worked to find the thermo-electric behavior of shape memory alloys[27]. A test rig similar to T. Georges test bench was used with 0.381 mm diameter wire. One way shape memory effect was implemented as a single shape memory alloy wire was used. Experiments were carried out at different applied stresses and the thermoelectric behavior was observed and analyzed.

2.6 Summary:

A lot of work has been done in last three decades regarding the thermo-electric behavior of NiTi shape memory alloy. NiTi SMA is instable and hard to control that’s why a feedback control of

SMA is still to be determined that gives us the relationship between the applied stress and the displacement of the NiTi wire, therefore the research still continues in this area.

Chapter 3

Test bench Development

3.1 Introduction:

Shape Memory alloys are characterized to find its thermo-electric properties. Much work and research have been done in this field which is already discussed in chapter 2. In order to find relation between stress, heating rate and the pre-loading, a test bench is developed on which experiments are performed.

In this chapter a brief description of test bench along with the properties of shape memory alloy wire (NiTi) is discussed. After that the characteristics of the linear actuator and the sensors used, that are Linear Variable Differential Transformer and Load cell, in this test bench are discussed.

3.2 Test Bench:

A test bench is developed in order to find the characteristics of NiTi shape memory alloy wire. The base frame is made of acrylic on CNC machine. The excess of the material in the middle is removed to make the test rig less heavy. A pair of bearing guides is used, one on each side, and is fixed on the acrylic base frame. These bearing guides provide strength to the bench and they are also helpful in guiding the moving plate on the rig. A central plate is fixed on these bearing guides with the help of the linear bearing at each end. This central plate is also made of acrylic.

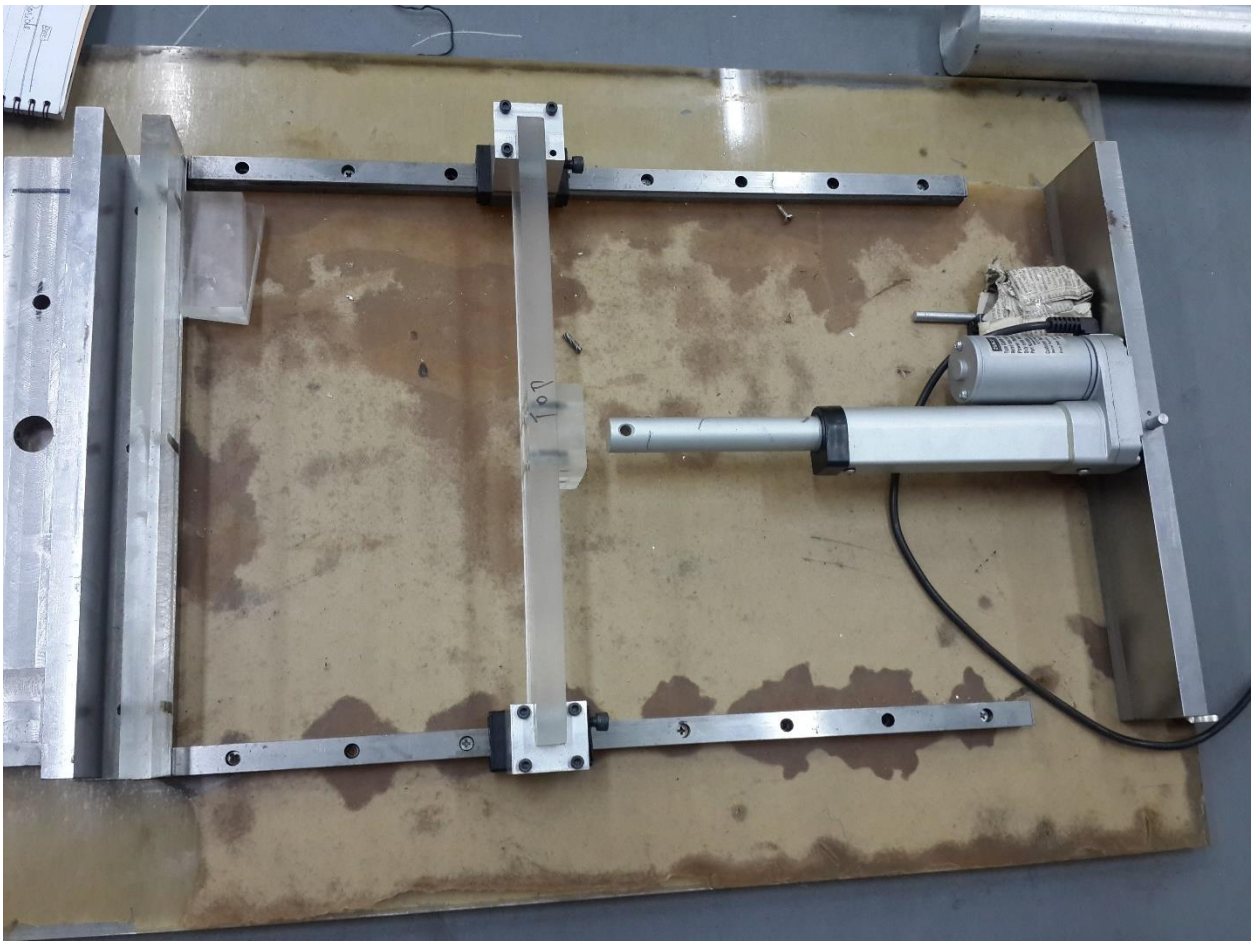

Fig. 3 Base of Test Bench with bearing guides, plates and the linear actuator

The stroke of the linear actuator is attached in the middle of one side of the central plate. This central plate is moved on the guiding bearing when the linear actuator moves forward or backward. The other end of linear actuator is attached to a fixed aluminum plate. A small rectangular piece of acrylic plate is screwed on the other side of the central plate in order to hold one end of the NiTi wire. Similarly the other end of NiTi wire is screwed to one end of the S-shaped load cell with a help of a gripper. This gripper is screwed in the load cell which is attached to the other aluminum fixed plate. The fixed plate on one end of the test bench, linear actuator, moveable plate, SMA wire, S-shaped load cell and the fixed plate on other side of the test bench all are concentric. So when the linear actuator moves forward or backward, the force is transmitted to the wire and in turn to the load cell that gives the reading of the force exerted by the linear actuator. A linear variable differential transformer, which is a position sensor, is attached to the moveable plate and it moves as the plate moves and gives the change in position of the SMA wire.

3.3 Linear Actuator:

A linear actuator of CAHB-10 series of SKF is used in the test bench. A labelled diagram of linear actuator is shown below.

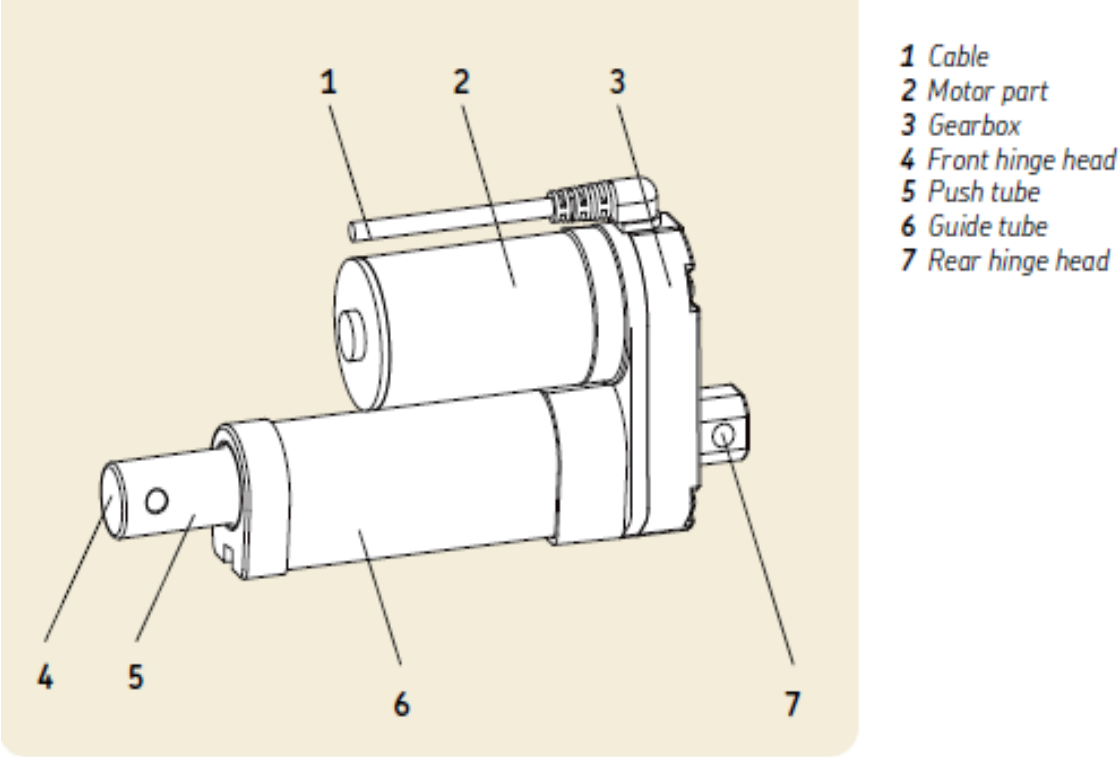

Fig. 4 Linear Actuator with parts labelled

The part 1 in the diagram shows the cable which is connected to the linear actuator. Motor is shown at 2 along with the gear box at 3. At 4, there is front hinge head which is used to attach the linear actuator to some support. The push tube is at 5 which moves forward or backward. Guide tube is shown at 6 and the rear hinge head is at 7 which is used to attach the rear of linear actuator to some support.

This linear actuator is fixed in the test rig with its front hinge head and rear hinge head. The rear hinge head is attached to the fixed plate made of aluminum. The front hinge head is attached to the acrylic moveable plate. The push tube of the linear actuator is used to move the acrylic moveable plate forward or backward.

Fig. 5 Linear Actuator attached at both ends on Test bench

3.3.1 Properties of the Linear Actuator:

The linear actuator used in the test bench is made of SKF and its model number is CAHB-10-B3A-100209-AAAAOA-000. The properties of the linear actuator are encoded in this model number.

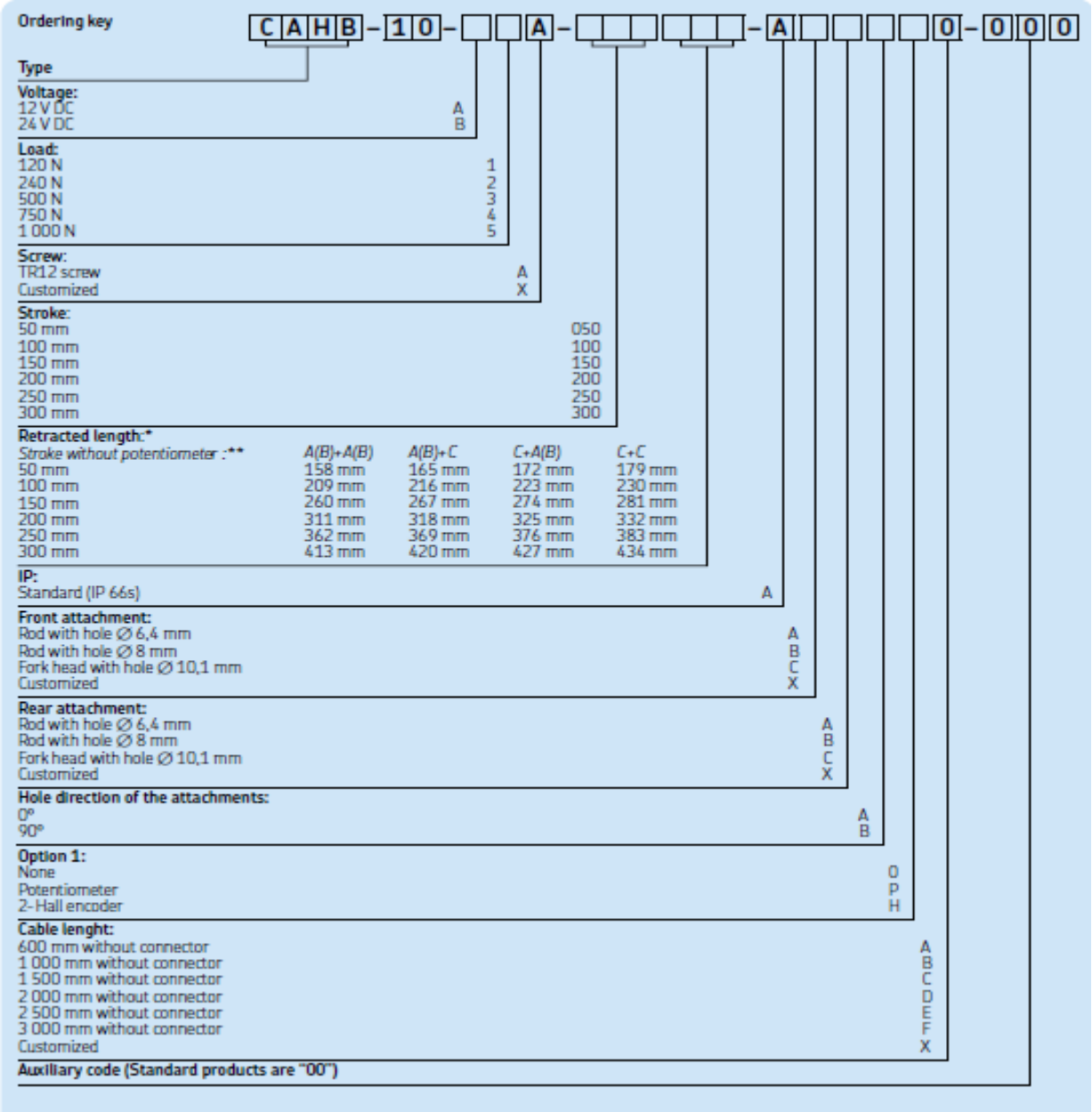

Fig. 6 Operating Key of Linear Actuator

CAHB -10 is the series of the linear actuator. B shows that the operating voltage of this linear actuator is 24 volts. 3 shows that the linear actuator can exert maximum of 500 N force. The next box in the model operating key shows the type of screw which would be used to attach the linear actuator to any support. TR 12 screw is the one in our case and it is shown by A in the operating key. The next three boxes in the operating key show the length of the stroke of the linear actuator which is 100 mm in our case and is shown by 100 in the operating key. The next three boxes in

the operating key show the retracted length of the linear actuator which is 209 mm in our case and is shown by 209 in the operating key. The next A shows the standard (IP 66s) of the linear actuator used in this test bench. The next three boxes in the operating key give the details about the holes at the front hinge head and the rear hinge head. Each of these three boxes is filled with A. The first two boxes show that the rod with hole diameter of 6.4 mm is there in the front attachment and the rear attachment of the linear actuator. A in the third box shows the hole direction in the attachment which is 0° in our case. The next box in the operating key shows whether the potentiometer and the 2-Hall Encoder is along with linear actuator or not. In this linear actuator which is used in the test bench is not provided with the potentiometer and the 2-hall encoder and it is shown by O in the operating key. The next box tells about the length of the cable attached and this box is filled with A which shows that the length of the cable is 600 mm without the connector. The last two boxes are filled with 00 which is the auxiliary code for the standard products.

The standard connections of the cables by which they should be connected to move the push tube forward or backward are shown in the figure below.

	Cable (Red)	Cable (Black)	Actuator (Standard)
I	-	+	Extending
II	+	-	Retracting

Fig. 7 Cable Connections

3.3.2 Benefits:

The benefits of SKF linear actuator are listed below.

1. Compact Design
2. Designed for harsh environment
3. Robust and Reliable
4. Integrated limit switches
5. Quite operation
6. Thermal protection

3.4 Linear Variable Differential Transformer:

Linear variable differential transformer (LVDT) is a position sensor which is used to find the exact position. LVDT is very sensitive to any movement and gives accurate reading.

Fig. 8 Linear Variable Differential Transformer (LVDT)

RS's new S-series range of displacement transducers gives a wide measurement range that is ±2.5 mm to ±150 mm. LVDT relies on the coupling of magnetic flux therefore it can have infinite resolution hence detecting the smallest fraction of the movement.

The general specifications for the S-series displacement transducers are as follows:

Description	LVDT Variants	Range
Storage Temperature	4-20 mA & DC variants	-20 °C to +85 °C
Operating Temperature	4-20 mA & DC variants	0 °C to 65 °C
Linearity	0.2% FSO	

Table 1 General Description of S-Series LVDT

3.4.1 Installation:

LVDT based transducers are a reliable and proven technology that is well established in all areas of manufacturing and control industries. The problems associated with the installation and working of LVDTs can easily be avoided if proper working is done during the initial design of the equipment and the right clamping method is attempted. LVDTs are inductive in nature and can be effected by the influence of magnetic field. The S-series displacement transducers decreases this magnetic effects as they have an integral magnetic screen. Similarly care should be taken while clamping the coil assembly. Screws should not be over tighten as this can cause damage to the LVDT body and this in turn can damage the integrity of the transducer.

LVDT used in this test bench is the S-series displacement transducer with the maximum stroke of 50 mm. The diameter of LVDT body is 19 mm and is made of stainless steel. It is installed along with the linear actuator to the moveable plate. A spring is fitted on the core of the LVDT which keeps the core extended upto the moveable plate. This spring works as a guided carrier for the core. SMA wire is attached to the other end of the moveable plate. LVDT gives the accurate reading when linear actuator moves in and out or the wire contracts or expands. LVDT relies on the coupling of magnetic flux therefore it can have infinite resolution hence detecting the smallest fraction of the movement.

3.4.2 Electrical Interface:

LVDT used in this test bench is the S-series displacement transducer. S-series LVDTs are available with different versions that are analogue, 4-20mA LVDT and the DC voltage LVDT. The one used in this test bench is the DC voltage LVDT. This displacement transducer gives us the DC voltage output.

Measurement Range	Output	Output
0-d mm	0-5 VDC	0-10 VDC
-d/2 to +d/2 mm	-5 VDC to +5VDC	-10 VDC to +10VDC

Table 2 Measurement Range for DC Voltage LVDT

An excitation voltage between 10 VDC to 30 VDC is required for this displacement transducer. The transducer output is electrically isolated from the input supply.

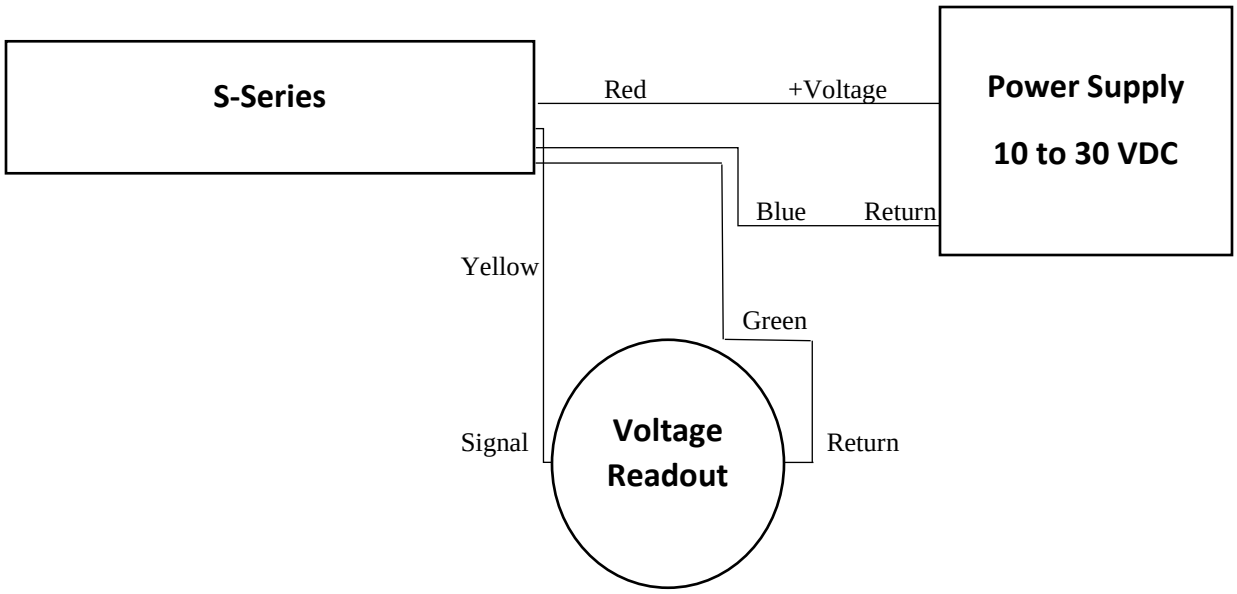

3.4.3 Calibration of LVDT:

The calibration of LVDT used in this test bench is done twice using LabVIEW 2015. The calibration is first done when the LVDT is not installed in the test bench. The second time LVDT is calibrated installed in the test bench. A calibration certificate is also provided by the manufacturer and the calibration graph is shown below.

Position (mm)	Output(V)	Error (%FSO)
-25.000	-4.9907	-0.093
-20.000	-3.9939	-0.061
-15.000	-3.0012	0.012
-10.000	-2.0047	0.047
-5.000	-1.0080	0.080
0.000	-0.0030	-0.030
5.000	1.0023	0.023
10.000	2.0024	0.024
15.000	3.0055	0.055
20.000	4.0001	0.001
25.000	4.9999	-0.001

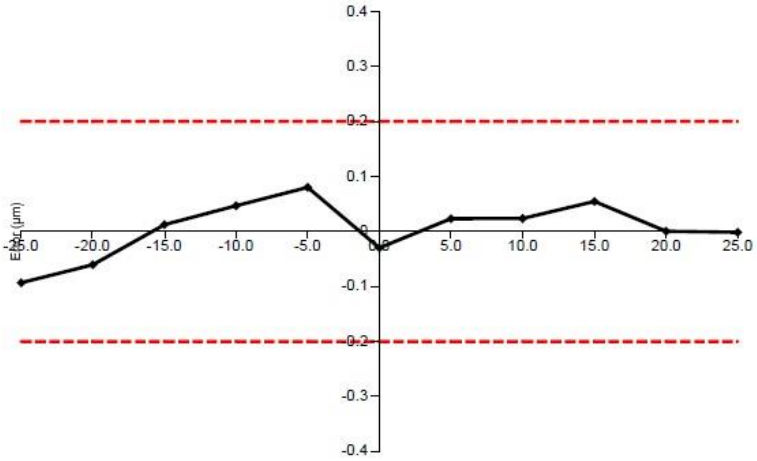

Fig. 9 Calibration chart of LVDT

This is the calibration chart provided by the manufacturer. The table shows the position of the LVDT core. The second column gives the output voltage and the third column shows the error. -25 mm is the position when the core is fully out and 25 mm is the position when the core is fully in. This LVDT operates in the DC voltage range from -5 V to +5 V. The maximum error shown by the LVDT is 0.093 (% Full Scale).

3.4.4 Benefits:

The main benefits of using RS's S-series displacement transducer are listed below.

1. <0.2% Linearity
2. Excellent measuring range for the body length
3. Multiple output options with integrated electronics
4. Large bore to core clearance for ease of installation
5. Excellent magnetic shielding
6. Absolute Positioning

3.5 Load Cell:

Load cells are highly accurate transducers that are used to measure the force or weight. Load cells are the integral part of any weighing system as they are highly accurate. There are many types of

load cells and they are selected depending upon the application. The factors upon which the selection of load cell depend are the accuracy class, capacity and the environmental conditions. The types of load cells are:

1. Bending Load Cells
2. Shear Load Cells
3. Compression Load Cells
4. Ring Torsion Load Cells

3.5.1 Principle of Load Cell:

Strain gauges are used in a load cell as the sensing elements. They are set in such a way that as the load is applied, strain is produced which is directly proportional to the load applied. The force or load applied is identified as a resistance change. The resistance of a strain gauge is given by

$$R = \frac{\rho L}{A}$$

When the strain gauge is in tension, the resistance increases whereas it decreases when the strain gauge is in compression. Four strain gauges are connected in Wheatstone bridge configuration. Sometimes the strain gauges are in a multiple of four and they are set in such a way that a small change in resistance is converted into the electrical signal. The output voltage of a Wheatstone bridge is given by

$$V_0 = \left(\frac{R_3}{R_3 + R_4} - \frac{R_2}{R_1 + R_2}\right) V_{ex}$$

3.5.2 S-Type Load Cell:

The load cell which is used in this test bench is the S-type load cell. It is made by Axis weighing system Japan and its model number is ALH-200. The capacity of this load cell is 200 Kg-f which is equal to 1961.33 N. The output of this S-type load cell is 2.00mV/v.

Fig. 10 S-Type Load Cell

S-type load cell can be easily identified by its shape as the name is suggesting. S-type load cell can be loaded both in tension or compression. If the output is rationalized, the S-type load cell can be used for single or multiple cell applications.

3.5.3 Calibration of Load Cell:

The calibration of load cell is done by hanging different weights and getting the corresponding voltages. The S-shaped load cell is calibrated when it was not installed in the test bench.

Fig. 11 Setup for calibration of Load Cell

LabVIEW 2015 software is used for this calibration process. Different weights ranging from 0 N to 150 N are added in the weighing pan with 10 N step rate. Corresponding voltages are recorded using the LabVIEW 2015 software. The resulting voltages ranges from 0.0085 mV to 0.154 mV. Later these values are added in the software when the load cell is installed in the test bench and experiments are performed.

3.5.4 Electrical Wiring:

The electrical wiring of the S-shaped load cell used in the test bench is that it has four wires. The red wire is to be connected to the positive of the excitation source whereas black of excitation source is connected to the black wire. Similarly green wire is connected to the positive signal while the negative signal is connected to the white wire. All of these four wires are connected to the DAQ assistant which is the medium through which communication is being established between hardware and the LabVIEW software. The required excitation voltage and the signal is provided by the DAQ assistant.

3.5.5 Benefits:

The main benefits of using S-shaped load cell are:

1. Bi-Direction (Tension/Compression)
2. Aluminum construction
3. Accurate reading
4. Easy Installation
5. Rationalized output

3.6 Thermocouple:

The sensor that is used to measure the temperature of the shape memory alloy wire is thermocouple. It is basically an electric device that measures the temperature by forming electrical junctions at different temperatures due to two dissimilar electric conductors. The thermocouple consists of two dissimilar conductors that give output in the form of voltage which is then interpreted in the form of temperature. Thermocouples are found in many different types and these types differ in their composition and the temperature measuring range.

3.6.1 K-Type Thermocouple:

The K-type thermocouple is used in this test bench to find the temperature of the shape memory alloy wire. It is most commonly used general purpose thermocouple. It is inexpensive and its measuring range is -200 °C to +1350 °C. Thermocouple is installed in the test rig in such a way that the tip of thermocouple is attached on the SMA wire with the help of adhesive and the other end is connected to the DAQ assistant that processes the signal and gives the output in the software.

3.6.2 Benefits:

The benefits of using thermocouple in the test bench instead of other temperature measuring devices are:

1. Inexpensive
2. Wide measuring range

3. Interchangeable
4. No excitation required

3.7 Shape Memory Alloy Wire:

The shape memory alloy wire used in this test bench is nitinol wire. It is basically nickel-titanium wire in which both nickel and titanium are in equal quantity. This nitinol wire is imported from Dynalloy Muscle wires USA. 0.5 mm diameter nitinol wire is screwed in the test bench and the total length used is 100 mm.

3.7.1 Heat Treatment of Nitinol Wire:

Prior to the experimentation, heat treatment of the nitinol wire is required. For this purpose, the wire is set in the required shape. It is the shape which is programmed in the wire and the shape memory alloy will come to this shape when it is heated above the transformation temperature. In the test bench, straight wire is to be used so that the force exerted by the wire remain uni-directional and exact reading of the force can be measured using the load cell.

The nitinol wire is set in the furnace in a straight linear shape. The maximum temperature of the furnace is set to 500 °C with the step rate of 10 °C. After reaching the maximum temperature that is 500 °C, the temperature is maintained for 5 minutes and then the wire is removed from the furnace and is quenched in water. This annealing process is necessary for the shape memory alloy as the wire can come back to its original form upon heating only if it is properly trained.

3.7.2 Installation of Nitinol Wire:

The total length of 100 mm is used in the test bench and the diameter of the wire is 0.5 mm. The wire is installed between the moveable plate and the load cell. One end of the wire is fixed with the moveable plate with the help of a shorter piece of acrylic plate which is screwed to the moveable plate. The other end of the wire is attached to the load cell with the help of a gripper.

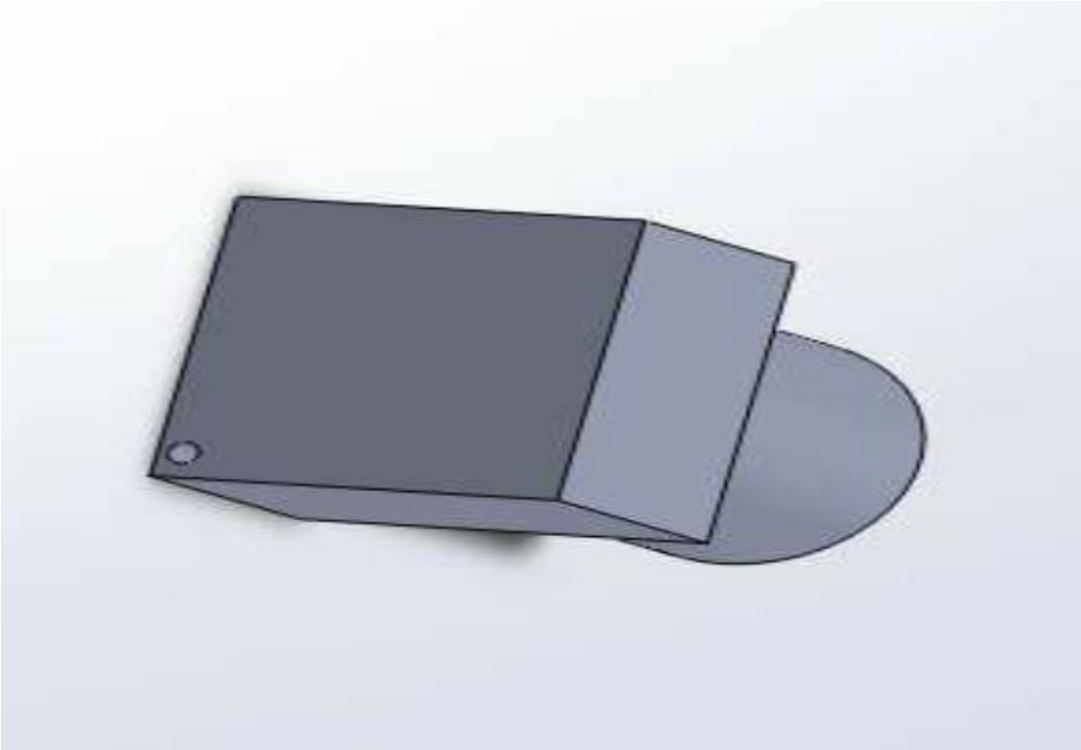

Fig. 12 Diagram of gripper

The rod like end of the gripper has threads. A sleeve of teflon has threads on its both inner and outer sides. This sleeve is screwed over the rod part of the gripper. The outer threads of the threaded sleeve are screwed inside the load cell. This sleeve is important to keep the load cell insulated from the nitinol wire. Teflon provides both electrical and heat insulation to the load cell.

CHAPTER 4

Software Development

4.1 Introduction:

The characterization of the shape memory alloy can be done using the test bench having different sensors which have already been discussed in chapter 3.The next step is the development of software with the help of which these sensors work and give the readings. The software should have been capable of regulating the whole test bench and inputs and outputs of actuator and sensors are controlled by it. The software used for this purpose is LabVIEW 2015.

In this chapter, a brief description of LabVIEW 2015 is given along with the knowledge about DAQ assistant which is used for the interfacing of actuator and sensors with the software.

4.2 LabVIEW 2015:

LabVIEW 2015 is integrated development software that is designed for measurement and control system purposes. It is specifically designed for engineers and scientists. It is based on graphical programming language. Further LabVIEW 2015 has a built-in IP for analysis of data and signal processing. It has an open architecture for integration of any hardware device to any software approach. LabVIEW is basically used for optimal solution meeting the requirements and solving the problems.

LabVIEW differs from other traditional programming languages like C, C++, and Java in a way that in LabVIEW programming is done graphically while in other languages programming is done in text. The programs that take weeks or months to write in other languages can be completed in hours in LabVIEW.

4.2.1 Virtual Instrument:

Virtual instrument also called VI is a LabVIEW program whose appearance and operation that mimics different instruments such as radio, oscilloscope, digital multimeters etc.
VIs of LabVIEW consists of three parts.

1. Front Panel
2. Block Diagram
3. Icon/Connector Panel

4.2.1.1 Front Panel Design:

A front panel of VI is the interactive user interface. The front panel of LabVIEW 2015 consists of controls (inputs) and indicators (outputs). Front panel contain controls palette in which controls and indicators of different data types such as numeric, string, And Boolean etc are available. Front panel also contain toolbar which is shown in Fig. 13.

The retrieval of controls (inputs) is carried out by acquiring from a device, reading directly from a file and manipulating controls. However we can output the data by displaying with indicators, logging to a file and outputting to a device.

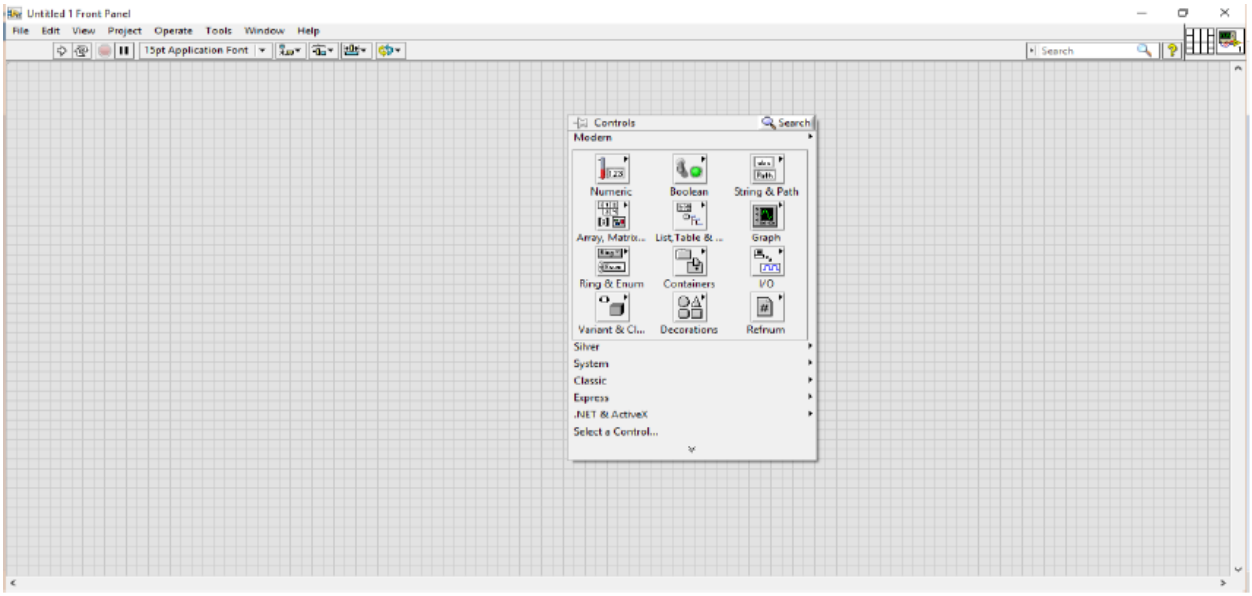

Fig. 13 Front Panel with Control Palette

The front panel that is made for this test bench is customised and there are many controls and indicators. Four waveform charts are used to show the results. Three of them show temperature, voltage and load which are basically the outputs of thermocouple, LVDT and load cell respectively. The fourth waveform chart shows the combined graph comprising of all the three graphs and allowing to compare them in the run time. There are also numeric indicators that show

the numeric value of temperature, load and position. Both position and the value of voltage output of LVDT are shown through the indicators. The output range of duty cucle of linear actuator is set by the controls and specific duty cycle is shown with the help of an indicator. Similarly the frequency is set with the help of a control. A control is used to set the set point for the load which has to be maintained by the linear actuator and for this purpopse PID Control is implemented on the linear actuator. A slider is also used for setting the set point in the LabView. The function of PID gains is already present in LabVIEW and it is used in implemenmting the PID control. The values of proportional gain,integral time and derivative time are set by hit and trial method. The front panel of software in shown in Fig. 14.

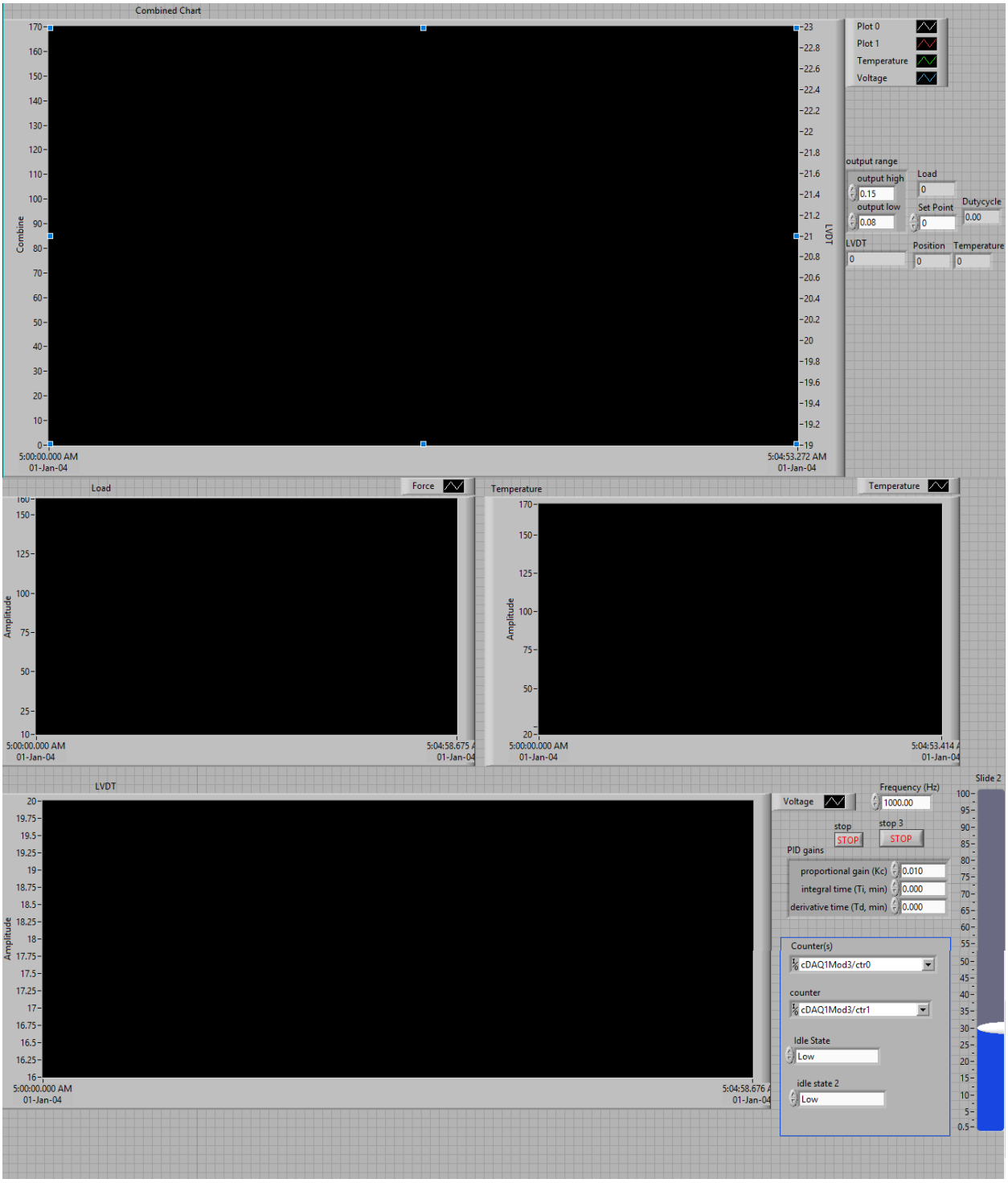

Fig. 14 Front Panel of software with control and indicators

The control panel of the software include all the control and indicators depicting the inputs and outputs of all the sensors which have already been discussed in chapter 3.

4.2.1.2 Block Diagram:

The objects in front panel appear as terminals in block diagram. Block diagram is also called the source code of a VI. It is the actual executable program. The block diagram has a function palette which has the following components

- Low level VIs
- Built-in functions
- Constants
- Program Execution Control Structures (For loop, while loop)

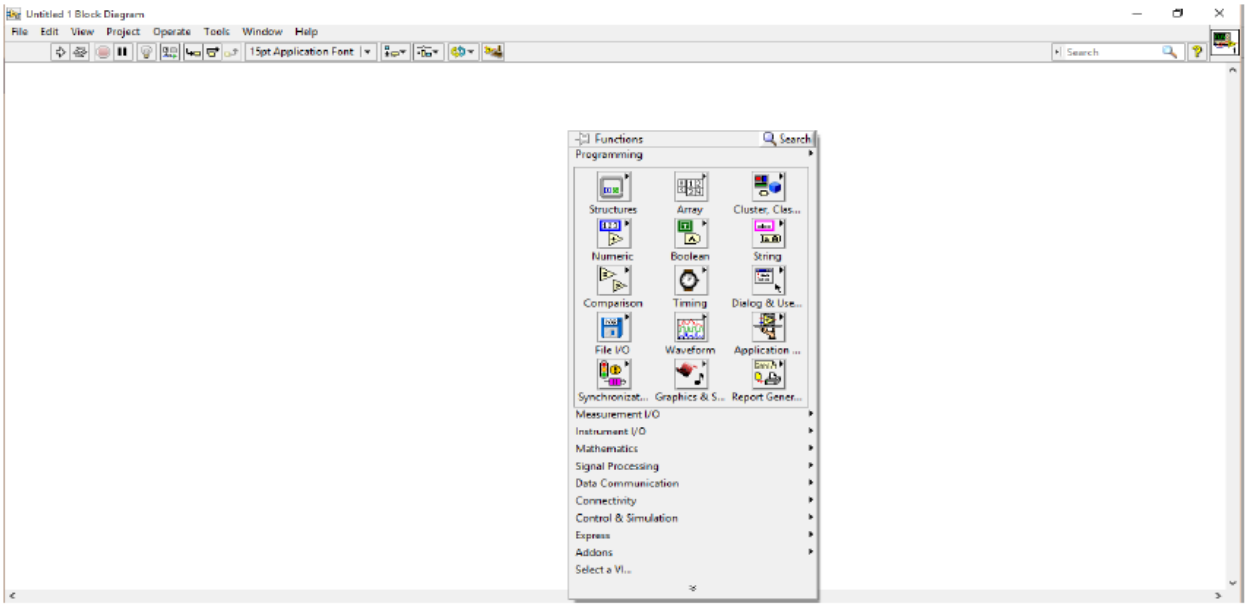

Fig. 15 Block Diagram with Function palette

In the block diagram, the code is written that executes and gives us the output on the front panel. PID is implemented in the block diagram and the two outputs are compared. The load cell output and the set point for the load, that has to be maintained, are compared. These are two different cases and the program executes differently.

Each input in the front panel appears as a terminal in the block diagram which is then used to program by using different mathematical operations and loops. The execution of the software for

the characterization of shape memory alloy wire depends upon the comparison of load cell output and the set point. Whether the linear actuator will move forward or backward it all depends on the difference and the software is well capable to make this decision. Case structure is used for this in the software and it selects the code according to the output of the comparison and executes the code. Case structures contain sub diagrams or cases.

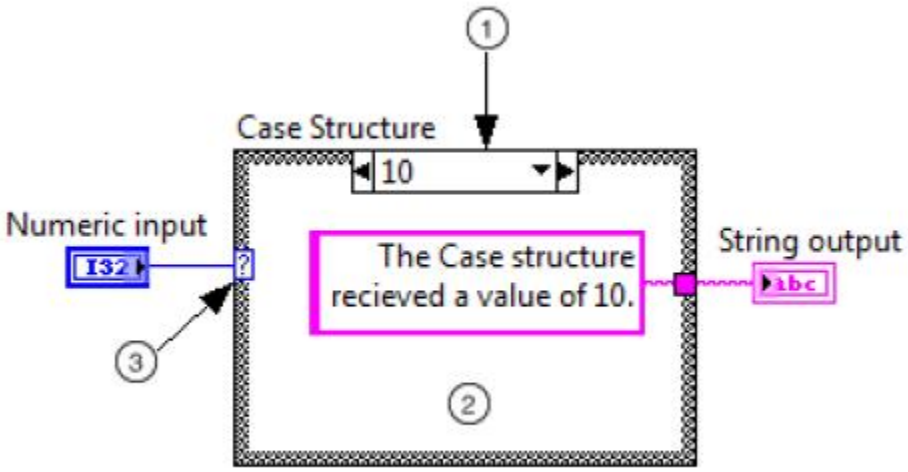

Fig. 16 Case Structure

1. Case Selector Label: It displays the value(s) for which the associated case executes.
2. Sub-diagram (case): It contains the code when the value that is connected to the selection terminal matches the value in case selector label.
3. Selector terminal: It is used to select the case that is to be executed which is based on the value of input data. The data can be Boolean, integer, string or error cluster. The data that is wired to the selector terminal determines the allowed cases that can be entered in the case selector label.

Sub diagrams can be added or removed by right clicking the edge of the case structure or selector label. Data is passed into and out of the case structure using tunnels which are automatically created when data is wired into or out of the case structure.

Execution of Code:

It is decided by the case structure whether the linear actuator will move forward or backward. A conditional terminal is wired with the output of comparison between load cell output and the set point for the load. If the load is greater than the set point, this means the load has to be decreased

and for that purpose, linear actuator will move forward. The block diagram of this software is shown below.

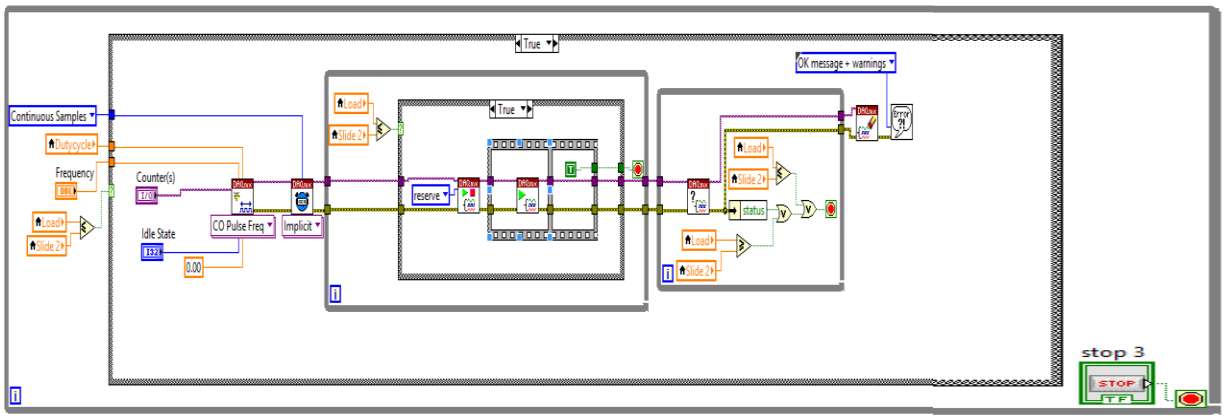

Fig. 17 Block Diagram for linear actuator moving forward (Load < Set Point)

In the above figure, the outer case structure is wired with the output of function indicating whether the load is greater than set point or not. If this condition is false, then the code for the false case will be executed i.e the linear actuator will move backward.

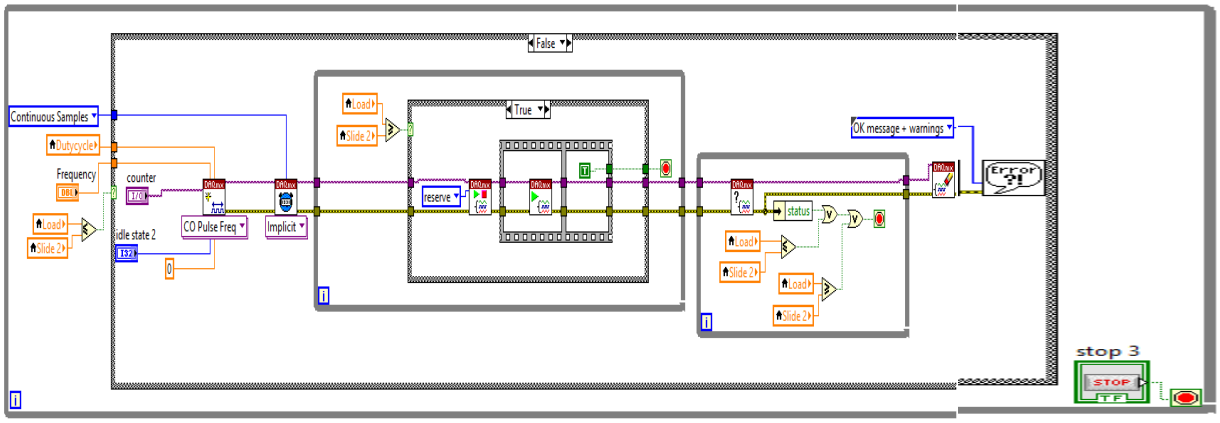

Fig. 18 Block Diagram for linear actuator moving backward (Load > Set Point)

Similarly there is another case structure inside the outer case structure. The conditional terminal of this case structure is also wired with the function output comparing whether the load is greater than the set point or not. If the load is greater than the set point, the true code executes which reserves the channel of the DAQ assistant for moving the linear actuator forward. The channel is unreserved if the output at the conditional terminal is false which allows the channel to get reserved

by the false code of the outer case structure and hence the linear actuator moves backward. Similarly the same check is applied on the false output of the outer case structure.

The below two figures show the false outputs for both true and false output of the outer case structure in which the channel of DAQ assistant is being unreserved.

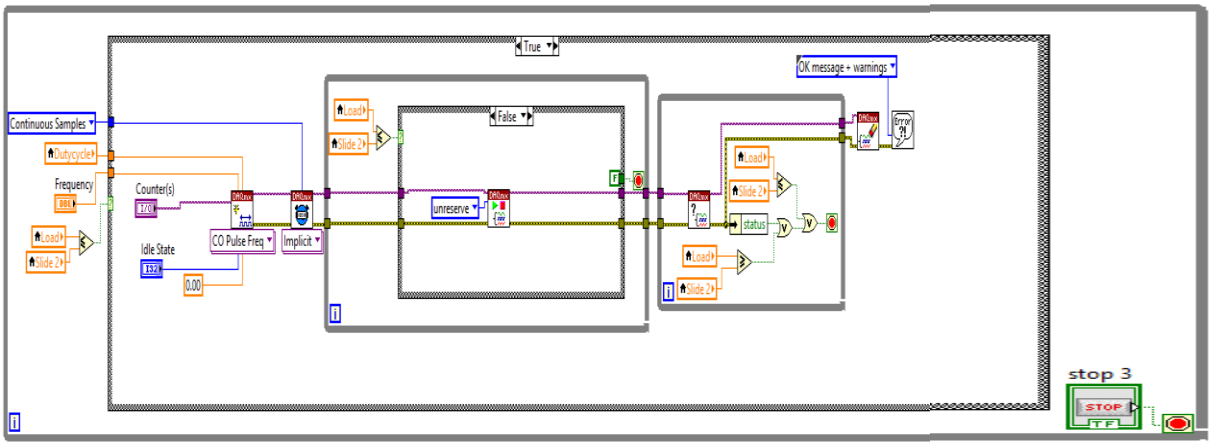

Fig. 19 Block Diagram for unreserving channel with true output

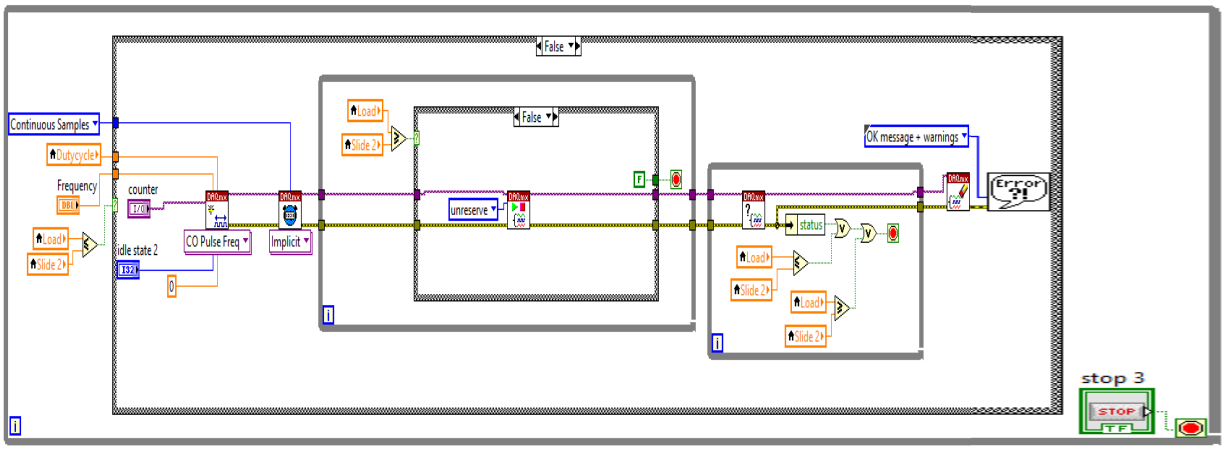

Fig. 20 Block Diagram for unreserving channel with false output

The DAQ assistant is basically the brain of this code and it regulates all of these case structures and functions. The code for the DAQ assistant is also there in the block diagram. All the outputs are controlled by the DAQ assistant with the help of the input terminals. PID control is also implemented in the block diagram. The output of the linear actuator is dependent on the PID control and it controls the duty cycle of the linear actuator within the range. PID control keeps the load on the wire close to the set point. Its block diagram is shown below.

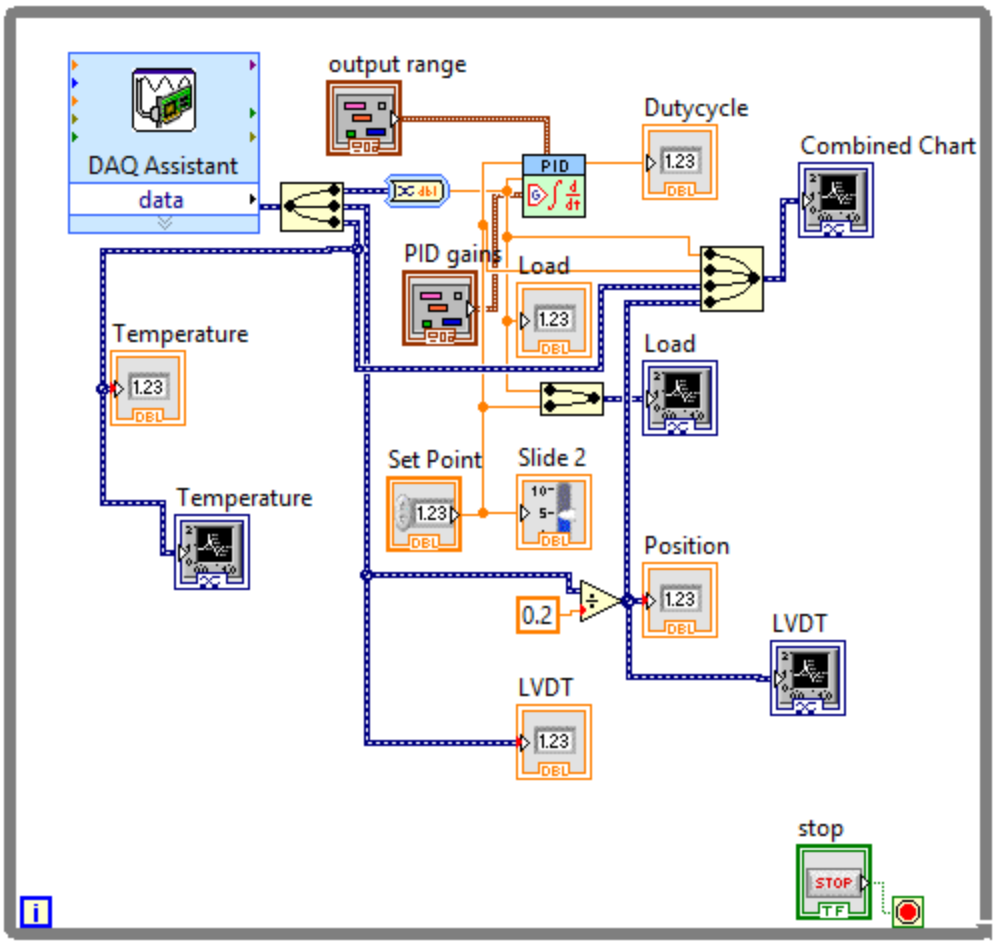

Fig. 21 Block Diagram for the DAQ Assistant

Chapter 5

Results and Experiments

5.1 Results:

After the development of software, the next step is to validate the displacement of the shape memory alloy during the experiment. For this purpose, experiments were performed on the test rig to obtain the displacement of the wire. Different instruments were used to get the displacement of wire while it is Joule heated. The results were then compared with the results of H.N Bhargaw. The experimental set up is shown below.

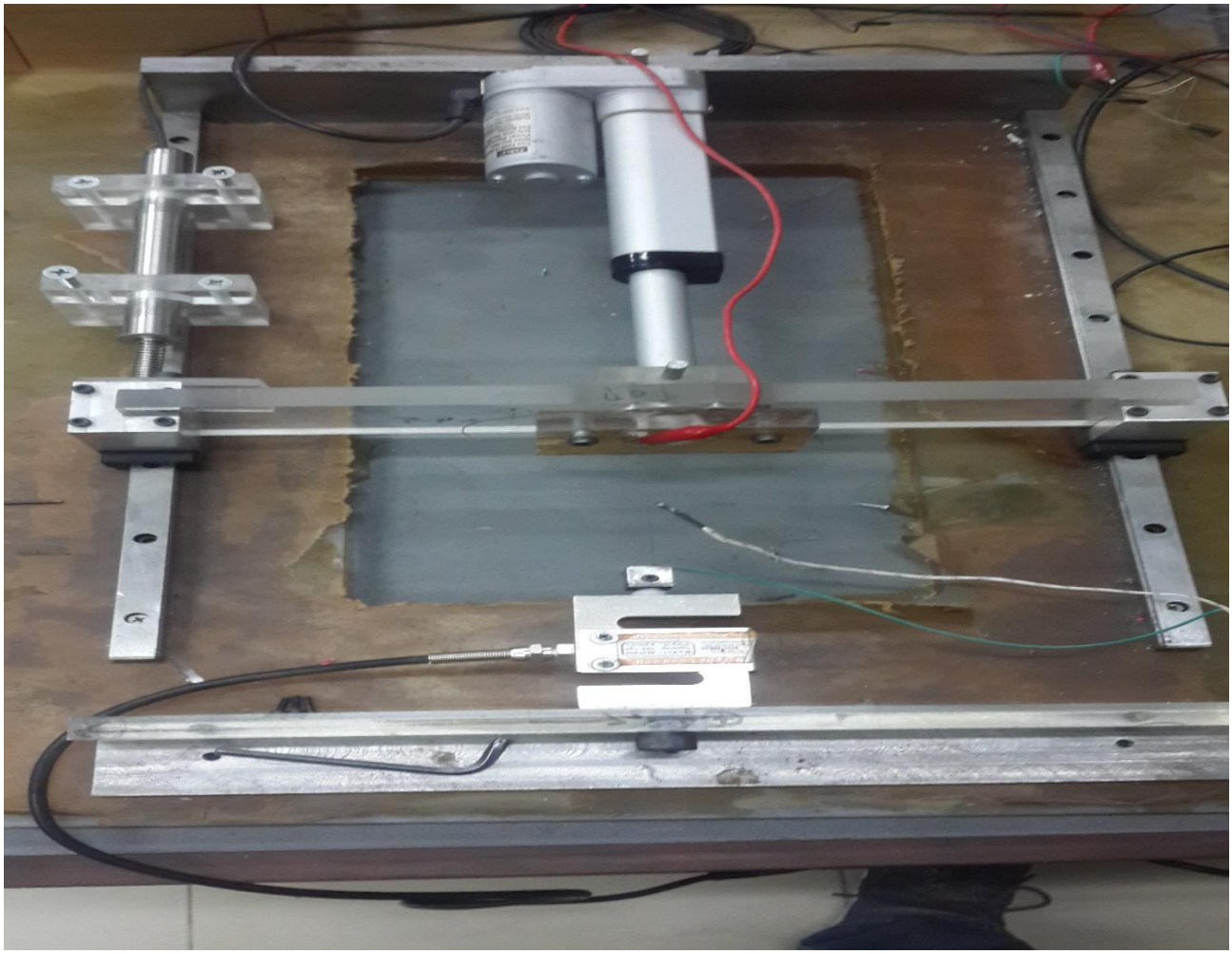

Fig. 22 Experimental set up of Test Bench

5.2 Comparison:

The shape memory alloy wire used by Bhargaw is of 0.381mm diameter and its length is 180 mm. Here the diameter of the wire is 0.5mm and length is 100 mm. The results obtained by Joule heating the wires are compared in the following table.

Properties of Wire	Output (H. N. Bhargaw)	Output (Software)
Diameter	0.381	0.5
Length	180	100
Displacement	7.8	3.24

Fig. 23 Comparison of Results

As the resistance of a wire is directly proportional to the length of the wire and is inversely proportional to the radius of the wire, therefore the difference in the displacement of the two outputs can be compensated in this regard. The actuation of the shape memory alloy wire is dependent on the resistance of the wire. The relationship of resistance of a wire is given by

$$R = \rho \frac{L}{A}$$

Therefore, the results of the software are validated with the H. N. Bhargaw results.

5.3 Experiments:

After the validation of software by comparing the results from software with that of H. N. Bhargaw, the next step is to find out the optimum current and heating rate at which maximum displacement can be obtained. For this purpose, experiments are performed at different currents and heating rates. Heating rate is changed by changing the duty cycle of the PWM which is heating the wire. The currents at which Joule heating is done are 0.4A, 0.7A, 1A and 1.3A. Similarly the duty cycles at which joule heating is done are 20%, 30%, 40%, 50%, 60% and 70%. Three experiments are performed at each set of values and then these results are compared to find the optimum heating rate and current.

The results of these experiments are shown in the following graphs.

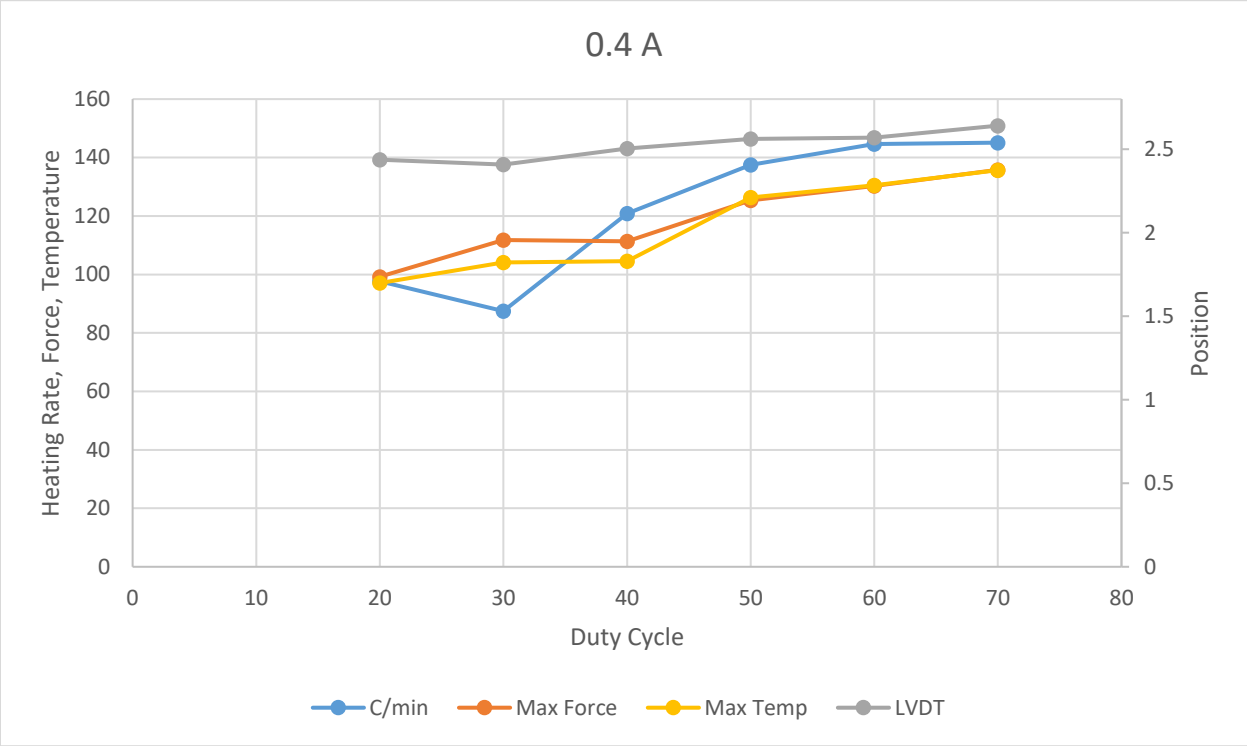

Fig. 24 Heating Rate, Force, Position and Temperature at different duty cycles & 0.4A

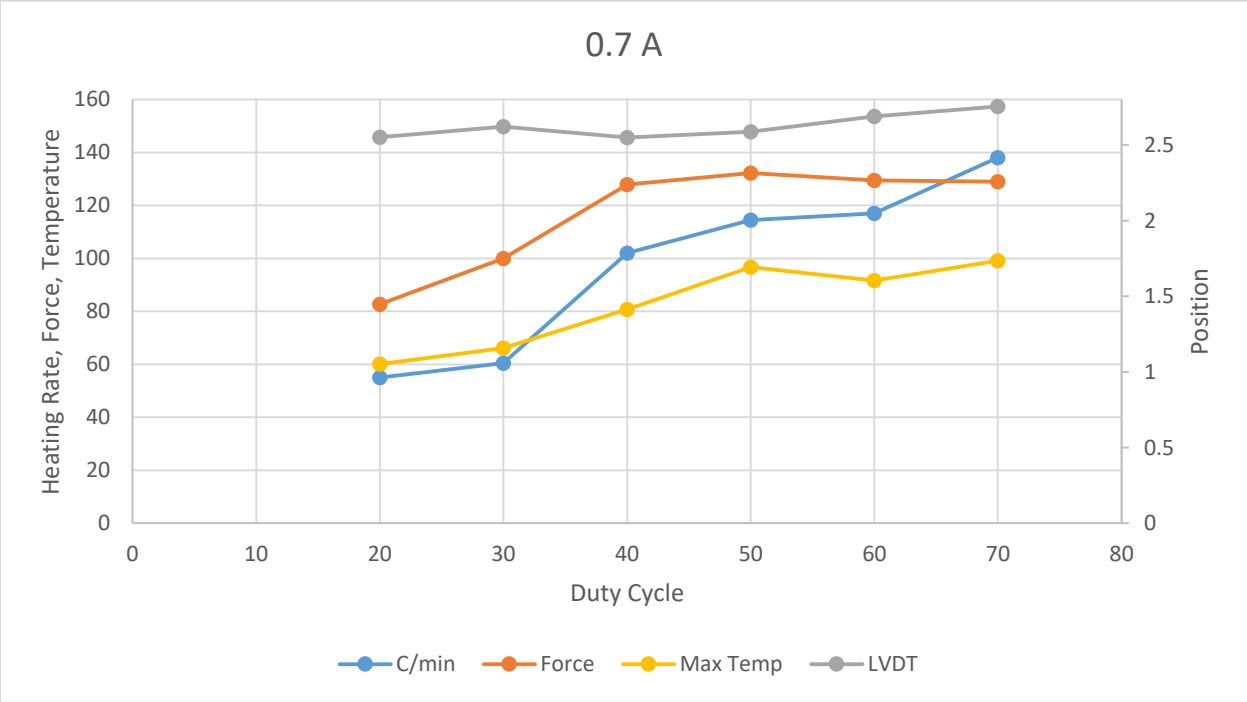

Fig. 25 Heating Rate, Force, Position and Temperature at different duty cycles & 0.7A

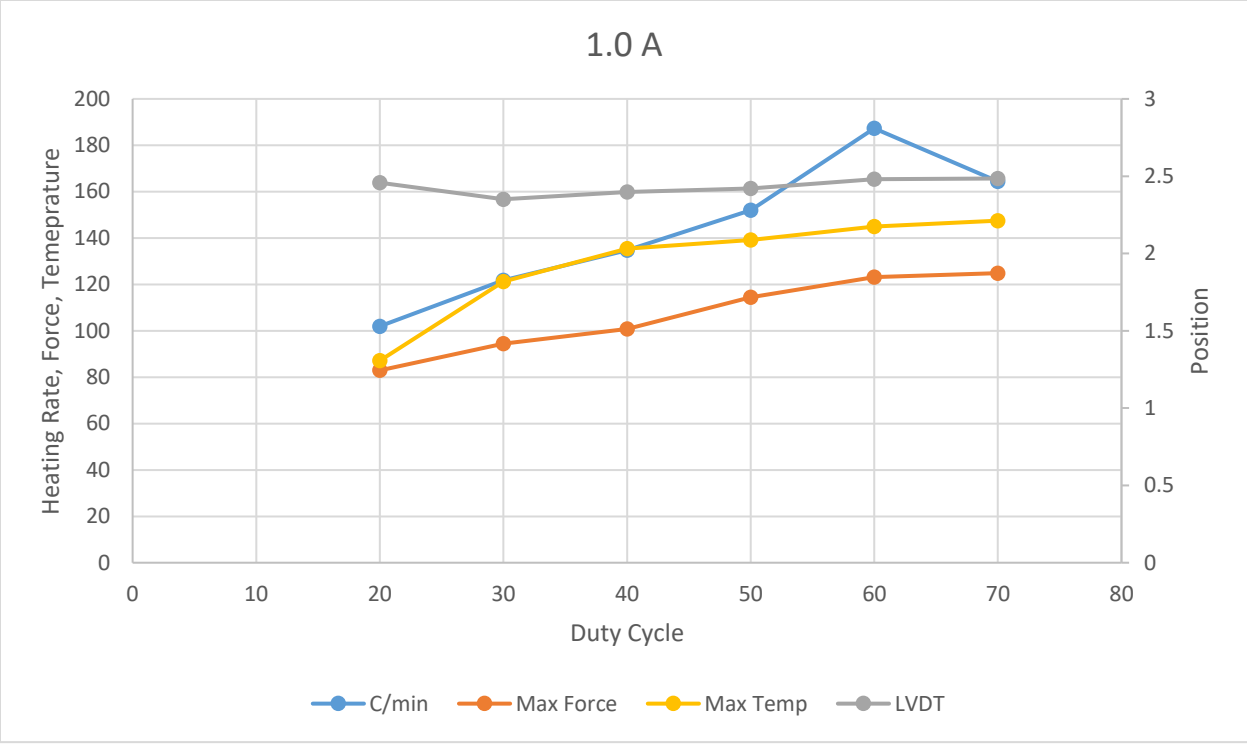

Fig. 26 Heating Rate, Force, Position and Temperature at different duty cycles & 1.0A

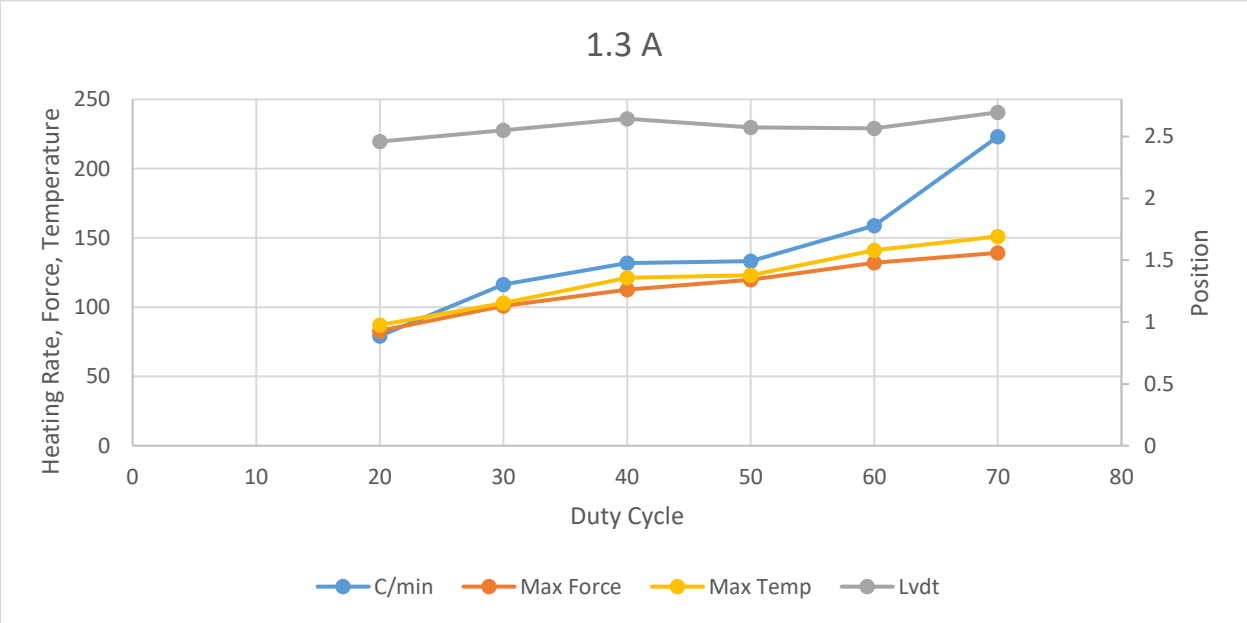

Fig. 27 Heating Rate, Force, Position and Temperature at different duty cycles & 1.3A

These above graphs show the results of 72 experiments. 18 experiments are performed for each set of duty cycle and current. The graphs show the change in heating rate, force, temperature and position of wire with respect to the duty cycle. It can be seen that maximum displacement is

obtained when experiments are performed at 0.7A current. It can also be observed from the graphs that rate of heating at constant current has almost no effect on the lateral displacement. Keeping in view these results, the optimum current selected is 0.7A and the heating rate is 140 °C/ min which is close to the one used by H.N. Bhargaw.

Once the heating rate and the optimum current is selected, the next step is to perform the experiments while keeping them constant and changing the pre-loading on the wire. Experiments are carried out on different values of stress .i.e. 10N, 15N, 20N, 30N and 45N. Three experiments are performed at each value of the stress and the results are then combined for each value in the form of graph. The values of temperature, position and force being applied by the wire against the time are shown in the graphs.

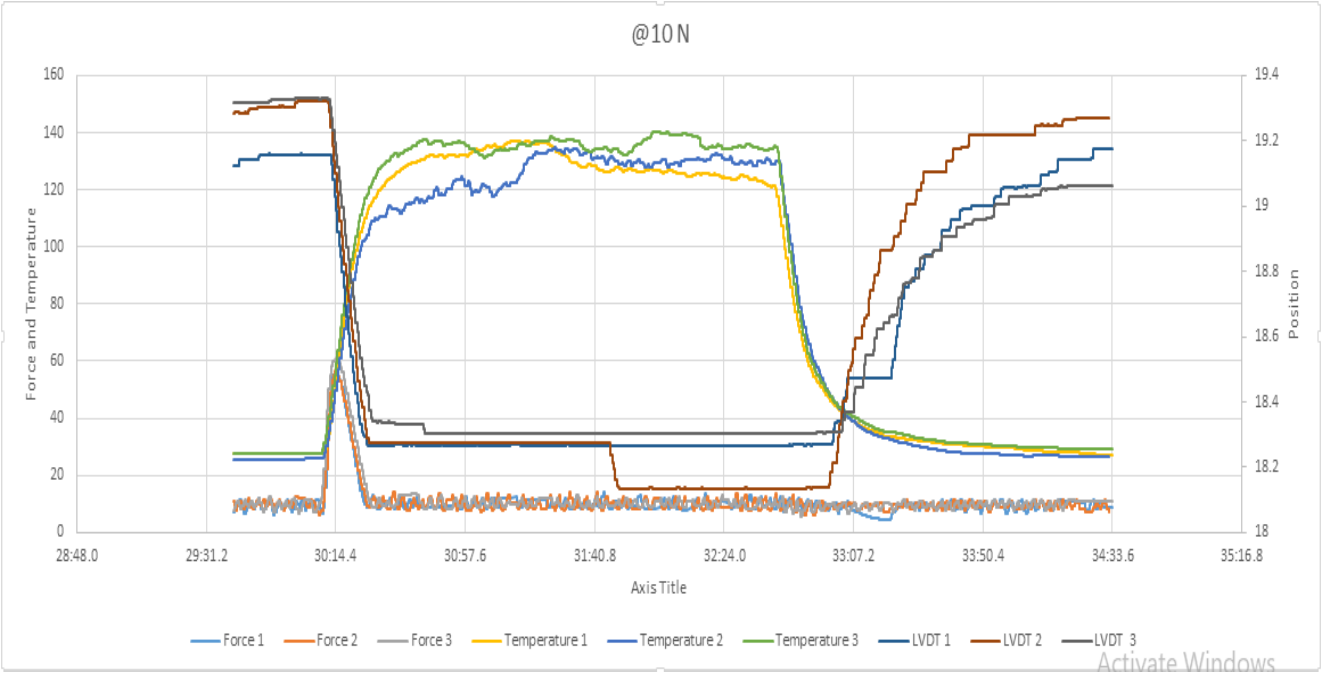

Fig. 28 Experiments @10N

The graph shows three experiments performed @10N stress. The values of force 1, temperature 1 and LVDT 1 comprises of one set of experiments. Similarly the other two sets show the other two experiments performed at 10N. The unsymmetrical lines showing the position of wire are because the value 10N is very small and it was difficult to overcome the sliding friction of the testing rig.

Similarly the following graphs show the experiments carried out at different pre-loaded stresses keeping the optimum current 0.7A and heating rate at 140 °C/min. Each of them showing three experiments performed at each value.

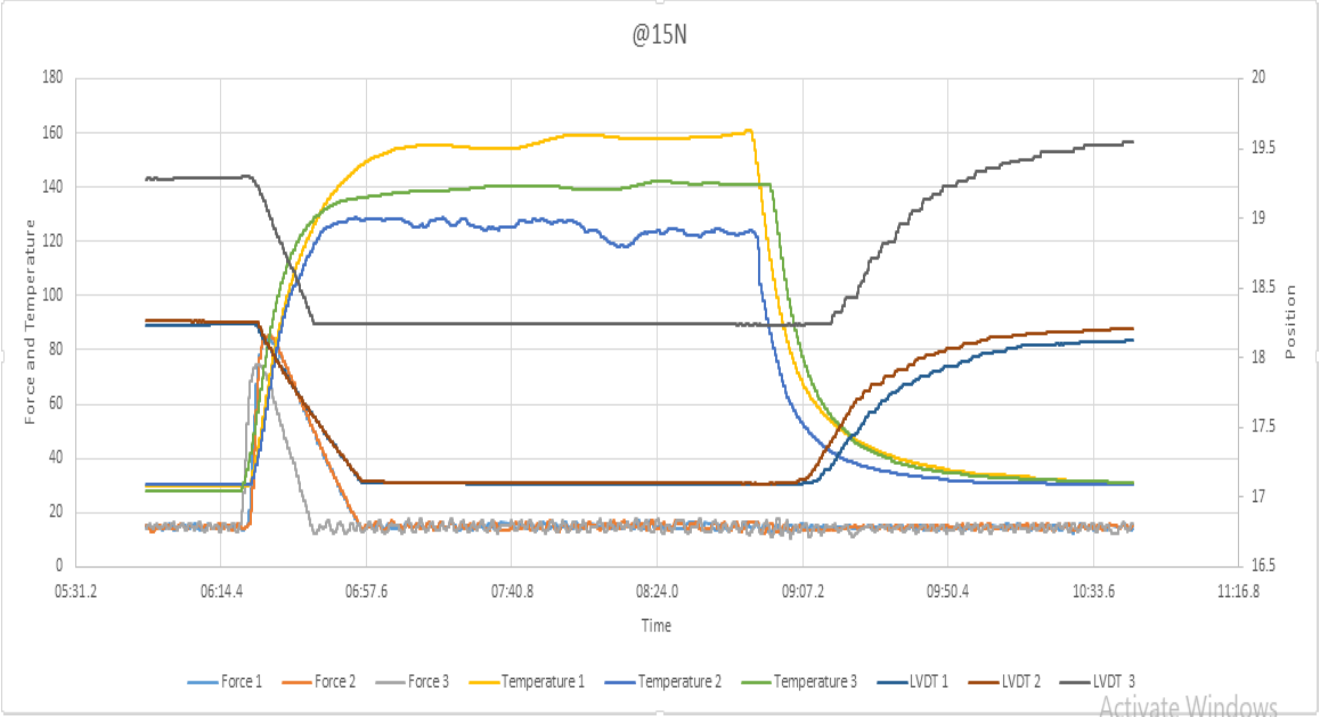

Fig. 29 Experiments @15N

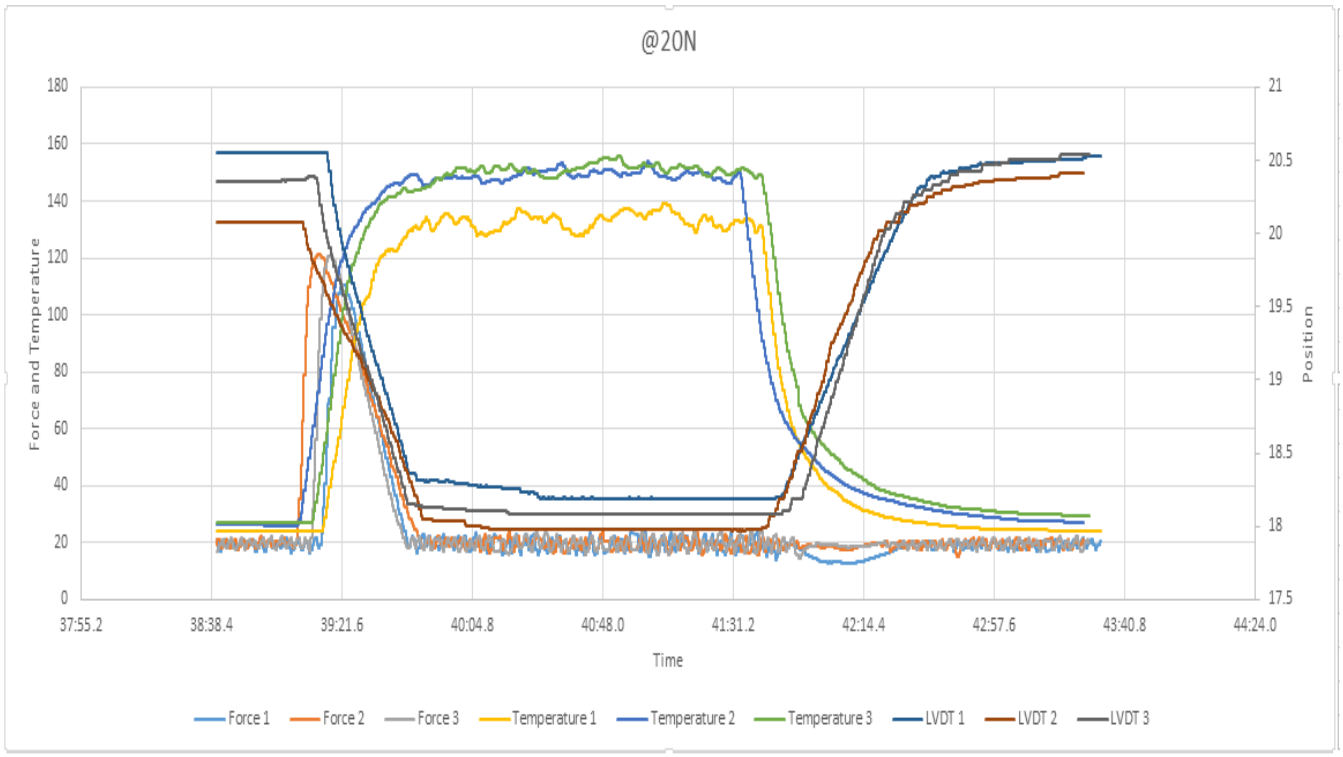

Fig. 30 Experiments @20N

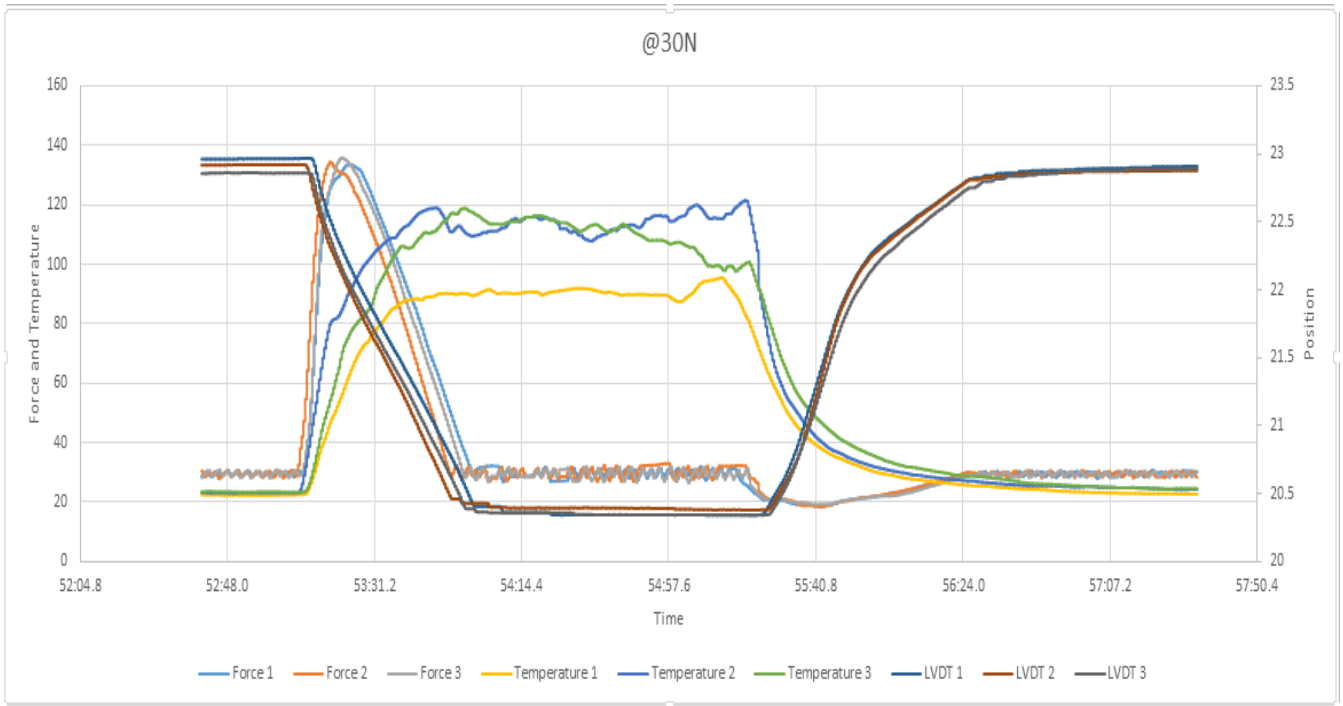

Fig. 31 Experiments @30N

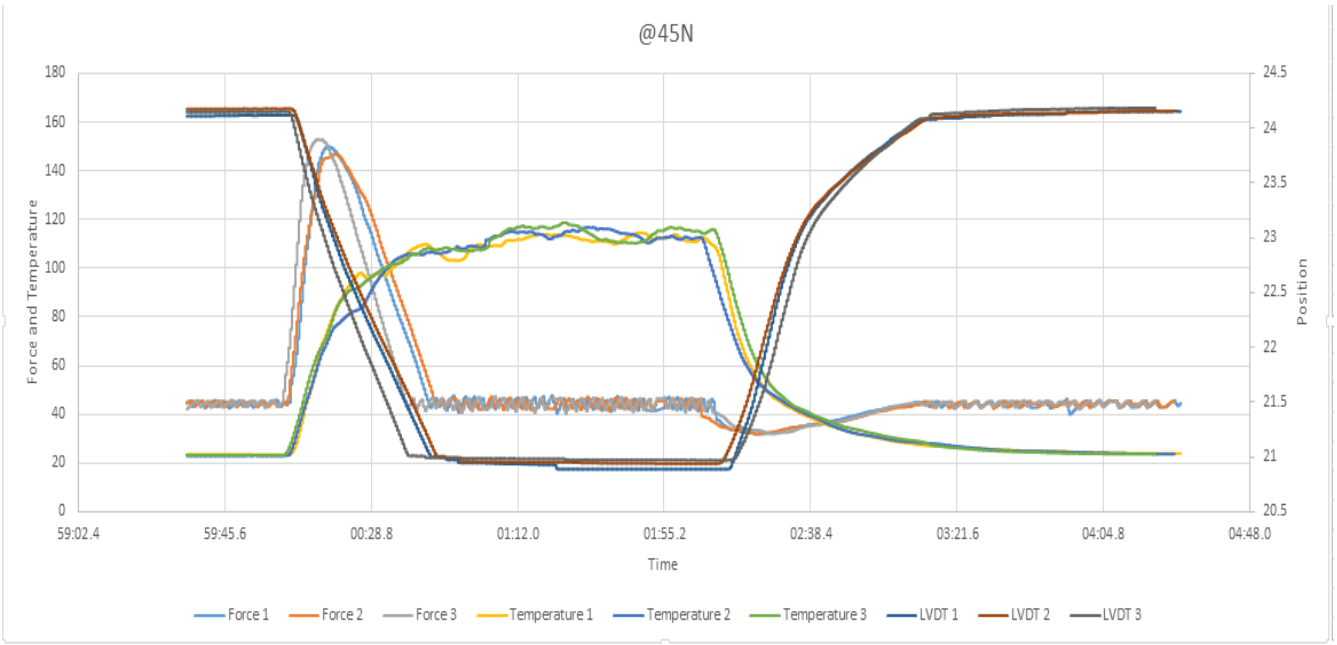

Fig. 32 Experiments @45N

The above graphs show the all the experiments that are performed at different pre-loaded stresses. Comparing them depicts that as the stress level on the wire is increased, the resulting displacement caused due to Joule Heating at constant current also increases. The displacement of the wire depends on the applied loading and increases with the increase in the pre-loading. This gives us the look up table with which we a relationship of displacement with respect to the pre-loaded stress. By carefully analyzing the look up table, we can have feedback system as well. If we know the displacement which is to be obtained, we can select the pre-loaded stress according to the look up table and we will have the same required displacement. This can be used in the application of Shape Memory Alloys as an actuator in different applications.

Chapter 6

Conclusions and Future Recommendations

6.1 Conclusions:

In this thesis, a test bench comprising of actuator and different sensors capable of performing experiment on Shape Memory Alloy wire and extracting the stress strain characteristics of the wire, development of software displaying these characteristics and applying PID control on the system are presented. The optimum current and heating rate are obtained by performing different sets of experiments and after finalizing these values, results are obtained by performing experiments at different stress levels. A linear actuator, LVDT, thermocouple, load cell and user friendly LabVIEW 2015 software are used for this experimentation.

A Shape memory alloy wire of 0.5mm diameter is imported. It is installed in the test bench and joule heated to perform experiments and obtain results. The results are compared with the results of H.N Bhargaw. The comparison is done and it is observed that the results are in accordance with those of H.N Bhargaw. Later on, different set of experiments are performed showing that the displacement of SMA wire increases with increase in the pre-loaded stress at constant current. Relationship between displacement and pre-loaded stress is also obtained.

6.2 Future Recommendations:

Following recommendations for future are presented.

- Implementing feedback control in the software.
- Using the Nitinol wire in some application where it can be used as an actuator.
- Using Shape Memory Alloy to make stent as it has already been developed.

References

1. Mohd Jani, J., et al., *A review of shape memory alloy research, applications and opportunities.* Materials & Design (1980-2015), 2014. **56**: p. 1078-1113.
2. Huang, W., *On the selection of shape memory alloys for actuators.* Materials & Design, 2002. **23**(1): p. 11-19.
3. Ölander, A., *An electrochemical investigation of solid cadmium-gold alloys.* Journal of the American Chemical Society, 1932. **54**(10): p. 3819-3833.
4. GRENINGER, A.B. and V. Mooradian, *Strain transformation in metastable beta copper-zinc and beta copper-Ti alloys.* AIME TRANS, 1938. **128**: p. 337-369.
5. Vernon, L.B. and H.M. Vernon, *Process of manufacturing articles of thermoplastic synthetic resins*. 1941, Google Patents.
6. Kurdjumov, G. and L. Khandros, *First reports of the thermoelastic behaviour of the martensitic phase of Au-Cd alloys.* Doklady Akademii Nauk SSSR, 1949. **66**: p. 211-213.
7. Chang, L. and T. Read, *Behavior of the elastic properties of AuCd.* Trans Met Soc AIME, 1951. **191**: p. 47.
8. Buehler, W.J., J. Gilfrich, and R. Wiley, *Effect of low-temperature phase changes on the mechanical properties of alloys near composition TiNi.* Journal of applied physics, 1963. **34**(5): p. 1475-1477.
9. Kauffman, G.B. and I. Mayo, *The story of nitinol: the serendipitous discovery of the memory metal and its applications.* The chemical educator, 1997. **2**(2): p. 1-21.
10. Otsuka, K. and C.M. Wayman, *Shape memory materials*. 1999: Cambridge university press.
11. Sun, L., et al., *Stimulus-responsive shape memory materials: A review.* Materials & Design, 2012. **33**: p. 577-640.
12. Morgan, N.B., *Medical shape memory alloy applications—the market and its products.* Materials Science and Engineering: A, 2004. **378**(1): p. 16-23.
13. Leo, D.J., et al. *Vehicular applications of smart material systems*. in *Smart Structures and Materials 1998: Industrial and Commercial Applications of Smart Structures Technologies*. 1998. International Society for Optics and Photonics.
14. Van Humbeeck, J., *Non-medical applications of shape memory alloys.* Materials Science and Engineering: A, 1999. **273-275**: p. 134-148.
15. Bil, C., K. Massey, and E.J. Abdullah, *Wing morphing control with shape memory alloy actuators.* Journal of Intelligent Material Systems and Structures, 2013. **24**(7): p. 879-898.
16. Brailovski, V., et al., *SMA actuators for morphing wings.* Physics Procedia, 2010. **10**: p. 197-203.
17. Furuya, Y., *Design and material evaluation of shape memory composites.* Journal of intelligent material systems and structures, 1996. **7**(3): p. 321-330.
18. Chemisky, Y., et al., *A constitutive model for cyclic actuation of high-temperature shape memory alloys.* Mechanics of Materials, 2014. **68**: p. 120-136.
19. Dönmez, B. and B. Özkan, *Design and Control of a Shape Memory Alloy Actuator for Flap Type Aerodynamic Surfaces.* IFAC Proceedings Volumes, 2011. **44**(1): p. 8138-8143.
20. Wilkes, K.E. and P.K. Liaw, *The fatigue behavior of shape-memory alloys.* JOM, 2000. **52**(10): p. 45-51.
21. Ma, N. and G. Song, *Control of shape memory alloy actuator using pulse width modulation.* Smart materials and structures, 2003. **12**(5): p. 712.
22. Duerig, T.W., K. Melton, and D. Stöckel, *Engineering aspects of shape memory alloys*. 2013: Butterworth-Heinemann.
23. Sun, L. and W. Huang, *Nature of the multistage transformation in shape memory alloys upon heating.* Metal Science and Heat Treatment, 2009. **51**(11): p. 573-578.
24. Leo, D.J., *Engineering analysis of smart material systems*. 2007: John Wiley & Sons.

25. Georges, T., V. Brailovski, and P. Terriault, *Characterization and design of antagonistic shape memory alloy actuators.* Smart Materials and Structures, 2012. **21**(3): p. 035010.
26. Song, H., E. Kubica, and R. Gorbet. *Resistance modelling of SMA wire actuators*. in *International workshop on smart materials, structures & NDT in aerospace conference*. 2011.
27. Bhargaw, H.N., M. Ahmed, and P. Sinha, *Thermo-electric behaviour of NiTi shape memory alloy.* Transactions of Nonferrous Metals Society of China, 2013. **23**(8): p. 2329-2335.